bioRxiv preprint doi: https://doi.org/10.1101/2020.06.30.179952; this version posted July 2, 2020. The copyright holder for this preprint (which was not certified by peer review) is the author/funder, who has granted bioRxiv a license to display the preprint in perpetuity. It is made available under aCC-BY-NC-ND 4.0 International license.

Tissue-resident macrophages regulate lymphatic vessel growth and patterning in the developing heart

Thomas J. Cahill[1,2,8], Xin Sun[1,2,8], Christophe Ravaud[1,2], Cristina Villa del Campo[1,2,3], Konstantinos Klaourakis[1,2], Irina-Elena Lupu[1,2], Allegra M. Lord[4], Cathy Browne[5], Sten Eirik W. Jacobsen[4], David R. Greaves[5], David G. Jackson[6], Sally A. Cowley[5], William James[5], Robin P. Choudhury[7], Joaquim Miguel Vieira[1,2,9,*] and Paul R. Riley[1,2,9,10,*]

[1]Burdon-Sanderson Cardiac Science Centre, Department of Physiology, Anatomy and Genetics, University of Oxford, Oxford OX1 3PT, UK.

[2]British Heart Foundation - Oxbridge Centre of Regenerative Medicine, CRM, University of Oxford, Oxford OX1 3PT, UK.

[3]Current address: Cardiovascular Development Program, Centro Nacional de Investigaciones Cardiovasculares, CNIC, 28029 Madrid, Spain.

[4]Karolinska Institutet, Department of Medicine Huddinge, Center for Hematology and Regenerative Medicine, Karolinska Institutet, Stockholm SE-14186, Sweden.

[5]Sir William Dunn School of Pathology, University of Oxford, Oxford OX1 3RE, UK.

[6]MRC Human Immunology Unit, Weatherall Institute of Molecular Medicine, John Radcliffe Hospital, University of Oxford, Oxford OX3 9DS, UK.

[7]Division of Cardiovascular Medicine, Radcliffe Department of Medicine, University of Oxford, Oxford OX3 9DU, UK.

[8]These authors contributed equally

[9]Senior author

[10]Lead Contact

[*]Correspondence: joaquim.vieira@dpag.ox.ac.uk (JMV), paul.riley@dpag.ox.ac.uk (PRR)

bioRxiv preprint doi: https://doi.org/10.1101/2020.06.30.179952; this version posted July 2, 2020. The copyright holder for this preprint (which was not certified by peer review) is the author/funder, who has granted bioRxiv a license to display the preprint in perpetuity. It is made available under aCC-BY-NC-ND 4.0 International license.

Running title: Macrophages and cardiac lymphatics

Keywords

Macrophages, hyaluronan, cell adhesion, cardiac lymphatics, coronaries, vessel growth and patterning.

Summary statement

Tissue-resident macrophages are indispensable mediators of lymphatic vessel formation during heart development and function to remodel the vascular plexus.

bioRxiv preprint doi: https://doi.org/10.1101/2020.06.30.179952; this version posted July 2, 2020. The copyright holder for this preprint (which was not certified by peer review) is the author/funder, who has granted bioRxiv a license to display the preprint in perpetuity. It is made available under aCC-BY-NC-ND 4.0 International license.

Abstract

Macrophages are components of the innate immune system with key roles in tissue inflammation and repair. It is now evident that macrophages also support organogenesis, but few studies have characterized their identity, ontogeny and function during heart development. Here, we show that resident macrophages in the subepicardial compartment of the developing heart coincide with the emergence of new lymphatics and interact closely with the nascent lymphatic capillaries. Consequently, global macrophage-deficiency led to extensive vessel disruption with mutant hearts exhibiting shortened and mis-patterned lymphatics. The origin of cardiac macrophages was linked to the yolk sac and fetal liver. Moreover, *Csf1r*$^{+}$ and *Cx3cr1*$^{+}$ myeloid sub-lineages were found to play essential functions in the remodeling of the lymphatic endothelium. Mechanistically, macrophage hyaluronan was found to be required for lymphatic sprouting by mediating direct macrophage-lymphatic endothelial cell interactions. Together, these findings reveal insight into the role of macrophages as indispensable mediators of lymphatic growth during the development of the mammalian cardiac vasculature.

bioRxiv preprint doi: https://doi.org/10.1101/2020.06.30.179952; this version posted July 2, 2020. The copyright holder for this preprint (which was not certified by peer review) is the author/funder, who has granted bioRxiv a license to display the preprint in perpetuity. It is made available under aCC-BY-NC-ND 4.0 International license.

Introduction

The cardiac vasculature, composed of the coronary circulation and lymphatic vessel network begins to develop from around mid-gestation, at approximately embryonic day (E)11.5 in the mouse embryo. Lymphatic endothelial cells (LECs) expressing the canonical lymphatic prospero homeobox 1 transcription factor (PROX1), vascular endothelial growth factor receptor 3 (VEGFR3) and lymphatic vessel endothelial hyaluronan receptor 1 (LYVE-1), first arise in the vicinity of the sinus venosus (dorsal side) and outflow tract (ventral side) of the murine heart at approximately E12.5 (Klotz et al., 2015). LECs then assemble into a primitive plexus that expands and remodels prenatally in the sub-epicardial surface along the base-to-apex axis and postnatally towards the myocardial layer, to form an extensive lymphatic system that drains lymph from the heart to enable optimal cardiac function (Flaht-Zabost et al., 2014; Klotz et al., 2015). Defects in lymphatic drainage are associated with heart disease, where an increase in tissue fluid content by as little as 2.5% can lead to a 30-40% reduction in cardiac output (Dongaonkar et al., 2010; Laine & Allen, 1991). Conversely, cardiac lymphatics respond to myocardial infarction by re-activating a lymphangiogenic gene expression programme and therapeutic stimulation of this process enhances resolution of macrophage-driven inflammation, promoting tissue repair (Klotz et al., 2015; Vieira et al., 2018). Together, these findings emphasize the importance of the cardiac lymphatic system and the need for a better understanding of the cellular and molecular mechanisms underlying its development.

The ontogeny of LECs integrating within the heart and other organ-based lymphatics has been the focus of a paradigm shift in recent times, with non-venous endothelial precursors now accepted as an additional source of the lineage (Eng et al., 2019; Gancz et al., 2019; Klotz et al., 2015; Martinez-Corral et al., 2015; Stanczuk et al., 2015; Stone & Stainier, 2019; Ulvmar & Makinen, 2016). The precise identity and origin of these non-venous LEC

bioRxiv preprint doi: https://doi.org/10.1101/2020.06.30.179952; this version posted July 2, 2020. The copyright holder for this preprint (which was not certified by peer review) is the author/funder, who has granted bioRxiv a license to display the preprint in perpetuity. It is made available under aCC-BY-NC-ND 4.0 International license.

precursors remains somewhat elusive, although genetic lineage tracing experiments have implicated the Tie2/PDGFB-negative transient embryonic hemogenic endothelium of the yolk sac and, more recently, second heart field-derived progenitors as contributing to cardiac lymphangiogenesis (Klotz et al., 2015; Lioux et al., 2020; Maruyama et al., 2019).

Macrophages are myeloid immune cells strategically dispersed throughout the tissues of the body with a vast functional repertoire and emerging plasticity that converges on normal homeostasis, and responses to pathology through mediating inflammation and repair. Macrophages were initially described in sites of physiological cell death within the bulbus cordis of embryonic chick and rat hearts, using light- and electron microscopy (Manasek, 1969; Pexieder, 1975; Sorokin et al., 1994). Subsequently *in vitro* experiments confirmed macrophages as phagocytic cells and, therefore, it was hypothesized that their primary role was to remove debris arising from cell death (Sorokin et al., 1994). Indeed, macrophages are specialised phagocytes with a classical role in engulfing and digesting dying or dead cells, cellular debris and pathogens. Macrophages are also responsible for cytokine production, and act as a source of pro (lymph-)angiogenic factors, such as VEGF-A, VEGF-C and VEGF-D which in turn support tumour growth, vascularisation and dissemination (Qian & Pollard, 2010). In addition to these classical roles in postnatal settings, macrophages have been implicated more recently in organogenesis during embryonic development and tissue regeneration after injury (Aurora et al., 2014; Theret et al., 2019), as well as in the maintenance of arterial tone through regulation of collagen turnover (Lim et al., 2018). In the embryo, macrophages arise initially from the extra-embryonic, transient yolk sac and subsequently from alternative sources within the embryo proper, including fetal liver-derived hematopoietic stem cells (HSC) (Ginhoux & Guilliams, 2016). Yolk sac-derived macrophages seed most tissue-resident niches, which are maintained through adulthood by self-renewal (e.g. microglia in the brain) or gradually replenished by HSC-derived, blood-

bioRxiv preprint doi: https://doi.org/10.1101/2020.06.30.179952; this version posted July 2, 2020. The copyright holder for this preprint (which was not certified by peer review) is the author/funder, who has granted bioRxiv a license to display the preprint in perpetuity. It is made available under aCC-BY-NC-ND 4.0 International license.

borne circulating monocyte intermediates, with both populations having distinct roles in tissue injury responses (Hoeffel et al., 2015; Lavine et al., 2014; Stremmel et al., 2018). In the developing heart, the outer mesothelial layer, the epicardium, has been proposed as an important signalling axis to recruit primitive yolk sac-derived macrophages to the subepicardial space (Stevens et al., 2016). The reported timescale for embryonic macrophage recruitment coincides with major morphological changes taking place in the growing heart, namely chamber septation, endocardial cushion formation and valve remodelling, myocardial growth and maturation, development of the electrical conduction system and formation of the coronary and lymphatic vasculature. As such, tissue-resident macrophages have been considered as potential key contributors to some of these processes *via* their functional roles in engulfing dying cells, releasing soluble cytokines, interacting with or recruiting progenitor cells and their potential to transdifferentiate into alternative cell types. Whilst a functional requirement has been identified for cardiac macrophages in valvular remodelling, normal conduction and coronary development (Hulsmans et al., 2017; Leid et al., 2016; Shigeta et al., 2019), there have been no reported roles during cardiac lymphatic development to-date. Given that macrophages contribute to adult lymphangiogenesis within inflammatory, wound healing and tumor microenvironmental settings (Qian & Pollard, 2010; Ran & Montgomery, 2012), as well as in the developing skin where they define nascent vessel calibre (Gordon et al., 2010), we sought to investigate the role of tissue-resident macrophages in the developing heart. Here, we demonstrate for the first time that macrophages are essential for cardiac lymphatic growth and remodeling. Macrophages colonized the developing heart prior to the initiation of lymphatic expansion, closely associating and interacting with the adventitial surface and leading edges of lymphatic vessels where they promote growth and fusion to ensure an adequate coverage over the subepicardial surface. Global genetic ablation of myeloid cells led to hyperplastic and shortened lymphatic vessels in the heart, which failed to

bioRxiv preprint doi: https://doi.org/10.1101/2020.06.30.179952; this version posted July 2, 2020. The copyright holder for this preprint (which was not certified by peer review) is the author/funder, who has granted bioRxiv a license to display the preprint in perpetuity. It is made available under aCC-BY-NC-ND 4.0 International license.

126 branch properly, and to a mis-patterning of the coronary blood vessels. Both extra- and intra-
127 embryonic hematopoietic sources were found to contribute to the tissue-resident macrophage
128 population, and fate mapping, based on canonical myeloid CSF1R and CX3CR1 markers,
129 identified overlapping lineages that contributed to the remodeling of the nascent lymphatic
130 network. In a co-culture model of human lymphatic endothelial cells with human induced
131 pluripotent stem cell-derived macrophages (hiPSC-macrophages), these cells closely
132 associated with tube-forming lymphatic endothelium where they induced sprouting,
133 replicating our *in vivo* findings. Mechanistically, a direct interaction between LECs and
134 hiPSC-macrophages was found to be dependent on macrophage hyaluronan, a linear
135 glycosaminoglycan composed of a repeating disaccharide unit of D-glucuronic acid and N-
136 acetyl-D-glucosamine, previously implicated in cell motility and adhesion during
137 angiogenesis and leukocyte trafficking through the lymph, respectively (Jackson, 2019;
138 Johnson et al., 2017; Lim et al., 2018; Savani et al., 2001). These findings significantly
139 increase our knowledge of (lymphatic) vascular biology and provide further insight into the
140 plasticity and diversity of tissue-resident macrophage function during development.
141 Mechanistic insight into the cellular interactions controlling lymphatic vessel formation is
142 potentially of more widespread interest in terms of understanding how to therapeutically
143 modulate macrophages and lymphatic growth during heart disease.
144

bioRxiv preprint doi: https://doi.org/10.1101/2020.06.30.179952; this version posted July 2, 2020. The copyright holder for this preprint (which was not certified by peer review) is the author/funder, who has granted bioRxiv a license to display the preprint in perpetuity. It is made available under aCC-BY-NC-ND 4.0 International license.

Results

Tissue-resident macrophages are closely associated with developing cardiac lymphatics

To investigate the earliest timepoint at which macrophages were first detected in the developing heart, we initially analyzed published single-cell RNA sequencing (scRNA-seq) data from whole heart at E9.25 and E10.5 (de Soysa et al., 2019; Hill et al., 2019) (Fig. S1). Whilst no macrophage cluster was detected at E9.25 (de Soysa et al., 2019), graph-based clustering followed by dimensionality reduction using Uniform Manifold Approximation and Projection (UMAP) (Becht et al., 2018) of the E10.5 dataset revealed 18 clusters corresponding to the major cardiac cell types (i.e. cardiomyocytes (CMs), endocardial cell (Endo), mesenchymal cells (Mes), epicardial cells (Epi), and second heart field cardiac progenitor cells (SHF)), which also included resident macrophages (Fig. S1A). The identity of the macrophage cluster was defined by the expression of key myeloid markers including receptors for the chemokine fractalkine (*Cx3cr1*) and cytokine colony-stimulating factor 1 (*Csf1r*) (Fig. S1B). Expression of the chemotactic ligand *Csf1* was detected exclusively in the Epi cluster, supporting the hypothesis that epicardial signaling underlies cardiac colonization and seeding of myeloid cells in the subepicardial compartment (Fig. S1B) (Stevens et al., 2016). To validate these findings, we made use of the *Cx3cr1-GFP* reporter mouse, which expresses enhanced GFP under the control of the endogenous *Cx3cr1* locus (Jung et al., 2000). We found that GFP^+ myeloid cells were present in the developing heart at E10.5 ahead of the onset of coronary and lymphatic vessel growth, being located on the sinus venosus and outer surface of the adjacent ventricular wall (Fig. S1C). Next, to assess a possible role in the formation of the cardiac lymphatic system, we measured the numbers and spatial distribution of tissue-resident macrophages in heart specimens at E12.5 and beyond (Fig. 1). Specifically, flow cytometric analysis of $Cx3cr1^{GFP/+}$ fetal hearts at E12.5, E14.5 and E16.5 combined with staining for the canonical macrophage marker EGF-like module-containing mucin-like

bioRxiv preprint doi: https://doi.org/10.1101/2020.06.30.179952; this version posted July 2, 2020. The copyright holder for this preprint (which was not certified by peer review) is the author/funder, who has granted bioRxiv a license to display the preprint in perpetuity. It is made available under aCC-BY-NC-ND 4.0 International license.

hormone receptor-like 1 (EMR1; henceforth, known as F4/80) (Hume & Gordon, 1983) revealed a distinct population of live singlet cells expressing both markers (Fig. 1A). Moreover, the $GFP^{+}F4/80^{+}$ macrophage count increased gradually from 297 ± 60 at E12.5 to 1018 ± 154 at E14.5 and 1569 ± 175 at E16.5 (E12.5 vs. E14.5, $p < 0.01$; E12.5 vs. E16.5, $p < 0.0001$; E14.5 vs. E16.5, $p < 0.05$; Fig. 1A), suggesting active recruitment and/or proliferation of macrophages throughout the time-course of cardiac development. To further characterize the macrophage population residing in the developing heart of *Cx3cr1*$^{GFP/+}$ mice, we performed whole-mount immunofluorescence staining using antibodies against the widely-expressed vascular marker endomucin (EMCN; restricted to capillaries and veins from E15.5 onwards (Brachtendorf et al., 2001)) and the lymphatic marker LYVE-1 that is also expressed in macrophages (Klotz et al., 2015; Lim et al., 2018) (Fig. 1B-M). At E12.5, GFP^{+} macrophages were found proximal to the sinus venosus (Fig. 1B,C) and in the outflow tract (Fig. 1D,E), prior to the onset of coronary and cardiac lymphatic vessel formation (Chen et al., 2014; Klotz et al., 2015). Indeed, only a primitive EMCN+ capillary network and $GFP^{+}LYVE\text{-}1^{+}$ macrophages, but no $LYVE\text{-}1^{+}$ lymphatics, were evident in the subepicardial surface at this stage (Fig. 1B-E). At E14.5, $GFP^{+}LYVE\text{-}1^{+}$ macrophages were more broadly dispersed in both dorsal and ventral surfaces of the developing heart and, in regions covered by vessels, macrophages were found to be in close proximity to, or in direct contact with, the nascent $EMCN^{+}$ coronary and $LYVE\text{-}1^{+}$ lymphatic vasculature (compare Fig. 1F,G with Fig. 1H,I). By E16.5, this spatial pattern of distribution was even more evident with $GFP^{+}LYVE\text{-}1^{+}$ subepicardial macrophages associating with the contiguous patent coronary and lymphatic networks (dorsal and ventral sides), notably alongside vessel branch junctions, leading ends (i.e. tips) and adventitial surface of vessel walls (Fig. 1J-M). Tissue-resident macrophages have previously been implicated in coronary vessel development and maturation (Leid et al., 2016), but their role in cardiac lymphatic vessel growth and remodeling has remained

bioRxiv preprint doi: https://doi.org/10.1101/2020.06.30.179952; this version posted July 2, 2020. The copyright holder for this preprint (which was not certified by peer review) is the author/funder, who has granted bioRxiv a license to display the preprint in perpetuity. It is made available under aCC-BY-NC-ND 4.0 International license.

undetermined. To investigate this further we initially validated the findings in *Cx3cr1*$^{GFP/+}$ mice, by investigating the developing cardiac lymphatics in transgenic *hCD68-GFP* mice, which report enhanced GFP in macrophages under the control of the human *CD68* promoter and enhancer sequences (Iqbal et al., 2014), combined with VEGFR3, LYVE-1 and PROX1 markers at E16.5 (Fig. 1N-U). Macrophages were found to be co-localized in the subepicardial space with VEGFR3^{+} lymphatic vessels and intimately associated with vessel branching and the leading edges of vessel sprouts (Fig. 1Q, white arrowheads and orthogonal views). Moreover, macrophages were detected bridging adjacent PROX1^{+} lymphatic tips to promote vessel fusion (Fig. 1U, white arrowheads), analogous to the previously reported cellular chaperone role for tissue-resident macrophages during blood vessel expansion in the developing hindbrain and postnatal retina (Fantin et al., 2010). Taken together, these studies reveal that tissue-resident macrophages colonize the embryonic heart prior to the formation of the main vascular networks and adopt a spatial distribution in close proximity to, and in contact with, the forming lymphatics.

Yolk sac-derived *Csf1r*$^{+}$ and *Cx3cr1*$^{+}$ myeloid lineages associate with lymphatic expansion

To define the origins of macrophages colonizing the developing heart during lymphatic vessel development, we employed genetic lineage tracing using *Csf1r*, *Flt3* and *Cx3cr1*-based mouse models, which in combination capture the main hematopoietic sources from early to mid-gestation, i.e. the transient hemogenic endothelium of the yolk sac and definitive HSCs within the fetal liver as well as the labelling of yolk sac-derived pre-macrophages (Benz et al., 2008; Ginhoux & Guilliams, 2016; Gomez Perdiguero et al., 2015; Kasaai et al., 2017; Stremmel et al., 2018) (Fig. 2). We initially employed the *Csf1r-Mer-iCre-Mer* transgenic model (henceforth referred to as, *Csf1r-CreER* mice) (Qian et al., 2011) crossed

bioRxiv preprint doi: https://doi.org/10.1101/2020.06.30.179952; this version posted July 2, 2020. The copyright holder for this preprint (which was not certified by peer review) is the author/funder, who has granted bioRxiv a license to display the preprint in perpetuity. It is made available under aCC-BY-NC-ND 4.0 International license.

with *R26R-tdTomato* reporter mice in which CRE recombinase activity downstream of *Csf1r* enhancer sequences was induced by tamoxifen pulsing at E8.5 (Fig. 2A-D). This phased induction ensured mapping of the spatiotemporal pattern of *Csf1r* activity in the transient yolk sac-derived erythro-myeloid progenitor (EMP) compartment (Gomez Perdiguero et al., 2015; Hoeffel et al., 2015). At E16.5, *Csf1r-CreER*$^{+}$ hearts pulsed at E8.5 revealed tdTomato^{+} cells in close proximity to, or in direct contact with PROX1-expressing LECs, with some of these cells exhibiting dual expression of tdTomato and PROX1 (Fig. 2B, white arrowhead). This modest, but reproducible contribution of the *Csf1r*$^{+}$ lineage to lymphatic endothelium (Klotz et al., 2015), supports the hypothesis that a subset of CSF1R^{+} EMPs emerge from the yolk sac at E8.5 to colonize the developing heart and acquire an LEC phenotype, before integrating into the nascent vasculature and contributing to the reported endothelial heterogeneity (Klotz et al., 2015; Lioux et al., 2020; Maruyama et al., 2019). Recently, a yolk sac-derived CSF1R^{+} EMP population was reported to contribute extensively to the endothelium of the nascent vasculature of the developing hindbrain (Plein et al., 2018). However, unlike in the brain, yolk sac-derived CSF1R+ EMPs colonizing the heart appear to give rise largely to tissue-resident macrophages seeding the subepicardial compartment.

To further characterize the ontogeny of cardiac macrophages, we analyzed the hearts of *Cx3cr1-CreER;tdTomato*$^{+}$ embryos, pulsed with tamoxifen at E8.5 (Fig. 2E-H). The *Cx3cr1-CreER* mouse drives expression of the fusion protein CRE-ERT2 (Cre recombinase-estrogen receptor) under the control of the endogenous myeloid-specific *Cx3cr1* locus (Parkhurst et al., 2013) and hence, tamoxifen pulse-chase from E8.5 was anticipated to capture the involvement of yolk sac-derived pre-macrophages (Ginhoux & Guilliams, 2016; Stremmel et al., 2018). Using this approach, we observed widespread contribution from extra-embryonic hematopoietic compartments (i.e. yolk sac) to the macrophage population residing in the

bioRxiv preprint doi: https://doi.org/10.1101/2020.06.30.179952; this version posted July 2, 2020. The copyright holder for this preprint (which was not certified by peer review) is the author/funder, who has granted bioRxiv a license to display the preprint in perpetuity. It is made available under aCC-BY-NC-ND 4.0 International license.

developing heart and closely interacting with the nascent PROX1^{+} lymphatic network. *Cx3cr1*$^{+}$ derived cells were exclusively macrophages; we did not observe any direct contribution of LECs within the forming lymphatic plexus (compare Fig. 2E-H with Fig. 2A-D).

To investigate a potential contribution from intra-embryonic definitive HSCs to the tissue-resident macrophage population in the developing heart, we used the *Flt3-CreERT2* mouse model (Benz et al., 2008). Upregulation of FMS-like tyrosine kinase 3 (FLT3; also known as fetal liver kinase 2 or FLK2) is critical for loss of self-renewal of definitive HSCs and *Cre* recombinase-driven by the *Flt3* locus has been demonstrated to label all progeny arising from HSCs (Boyer et al., 2011). At E16.5, *Flt3-CreERT2*$^{+}$ hearts pulsed at E13.5 and E15.5 to maximize recombination efficiency resulted in tdTomato^{+} cells residing in close proximity to, or in direct contact with, PROX1^{+} lymphatic vessels on the sub-epicardial surface (Fig. 2I-L), indicating a contribution from the definitive HSC compartment in the fetal liver to the macrophage population residing in heart at later stages of fetal development. Again, as for the *Cx3cr1*$^{+}$ lineage, no direct contribution to cardiac lymphatic endothelium was observed.

Macrophages are required for growth and branching of the cardiac lymphatic network

Our data suggest that yolk sac-derived myeloid lineages, defined by the activity of *Csf1r* and *Cx3cr1* gene expression, migrate to the heart and give rise to macrophages which seed the outer surface of the ventricular wall and interact closely with the neighboring lymphatic vessel network that develops from E12.5 onwards. To determine the functional requirements for these tissue-resident macrophages, we first investigated cardiac lymphatic development in a mouse model deficient for the essential ETS domain-containing transcription factor PU.1 (Fig. 3). *Pu.1* knock-out mice die around birth due to a severely underdeveloped immune

bioRxiv preprint doi: https://doi.org/10.1101/2020.06.30.179952; this version posted July 2, 2020. The copyright holder for this preprint (which was not certified by peer review) is the author/funder, who has granted bioRxiv a license to display the preprint in perpetuity. It is made available under aCC-BY-NC-ND 4.0 International license.

system, including a lack of myeloid cells (McKercher et al., 1996; Scott et al., 1994). The number of myeloid cells and macrophages in the developing hearts of *Pu.1*-null mice was determined by flow cytometry for the expression of the pan-leukocyte CD45, myeloid CD11b and macrophage F4/80 markers, and found to be significantly reduced compared to control littermate embryos ($CD45^+CD11b^+$ myeloid cells: 1.35 ± 0.25% vs. 0.02 ± 0.008% of all live cells, $p < 0.01$; $CD45^+CD11b^+F4/80^+$ macrophages: 85.4 ± 2.77% vs. 0.0 ± 0.0% of all live cells, $p < 0.0001$; Fig. S2A-D). As a consequence, cardiac lymphatic growth and patterning was observed to be severely disrupted in $Pu.1^{-/-}$, compared to control littermates at E16.5; with mutant hearts exhibiting hyperplastic and shortened LYVE-1^+ vessels (vessel length: 12536 ± 1155 μm vs. 7231 ± 734.8 μm; $p < 0.01$), as well as a significant reduction in the number of junctions (i.e. branchpoints; co, 254.2 ± 32.77 vs. $Pu.1^{-/-}$, 104.0 ± 10.52; $p < 0.01$) and overall plexus complexity; indicative of a sprouting/branching defect (Fig. 3A-J). A similar phenotype was observed at E19.5, before the onset of embryo demise at perinatal stages (Fig. 3K-T), thus excluding a developmental delay in lymphatic expansion in mutant versus littermate controls. Heart morphology in *Pu.1*-deficient embryos appeared grossly normal, with no evident defects in growth, cardiac septation or compaction of the myocardial layer (Fig. S2E,F), hence ruling out the possibility of a secondary cardiac phenotype contributing to the observed lymphatic defects. However, coronary blood vessel growth and patterning were mildly affected, with null-hearts displaying an overall reduction in subepicardial capillary vessel length and junction number (Fig. 4A-J), as well as exhibiting extra branches of main $EMCN^+$-coronary veins (Fig. 4E, white asterisk), compared to control littermates at E16.5. The mis-patterning of $EMCN^+$- coronary veins was still evident in *Pu.1*-deficient hearts at E19.5 (Fig. 4K-R, white asterisks in O and Q), whereas the coronary capillary vessel length and junction density were restored to equivalent levels as control littermate hearts (Fig. 4S,T).

bioRxiv preprint doi: https://doi.org/10.1101/2020.06.30.179952; this version posted July 2, 2020. The copyright holder for this preprint (which was not certified by peer review) is the author/funder, who has granted bioRxiv a license to display the preprint in perpetuity. It is made available under aCC-BY-NC-ND 4.0 International license.

In a previous study, macrophages in the skin were shown to define dermal vessel caliber by regulating lymphatic endothelial cell proliferation (Gordon et al., 2010). However, we did not observe any gross changes in LEC proliferation in *Pu.1*-null hearts, compared to control littermates at E16.5 (Fig. S2G-N), suggesting inherent differences across organ-specific lymphatic beds. The latter is supported by the emerging recognition of heterogeneity across the lymphatic vascular system and the existence of distinct origins for sub-populations of LECs (Ulvmar & Makinen, 2016).

To confirm a functional role for macrophages in cardiac lymphatic development and to exclude confounding factors arising from the indiscriminate targeting of immune cell development and potentially contributing to the severity of the phenotype in a *Pu.1*$^{-/-}$ background, we analyzed cardiac lymphatic development in mice expressing cytotoxic diphtheria toxin A (DTA) under the control of *Csf1r-CreER* and pulsed with tamoxifen at E12.5 (henceforth, *Csf1r-CreER;R26R-DTA*). DTA activation at E12.5, rather than E8.5 was chosen here to enable normal cardiac seeding by yolk sac macrophages. At E16.5, lymphatic vessel growth was disrupted and the number of vessel junctions was significantly reduced, compared to control littermate samples (vessel length: 21493 ± 1050 μm vs. 15940 ± 1507 μm; $p < 0.05$; number of junctions: 237 ± 23.27 vs. 107.0 ± 21.37 μm; $p < 0.01$; Fig. 5A-J). Moreover, a mild phenotype was identified during the development of the EMCN+ coronary vessels, with evident mis-patterning of the main coronary veins (Fig. 5K-T; white asterisk in O), phenocopying the (blood) vascular defects observed in *Pu.1*-deficient hearts (compare Fig. 5O with Fig. 4E). Therefore, ablation of the *Csf1r*$^{+}$ lineage, concurrently with the onset of cardiac lymphatic development, recapitulated some of the vascular phenotypes (lymphatic and blood endothelium) observed in *Pu.1*-null embryos, supporting a functional requirement for yolk sac-derived macrophages in cardiac lymphatic expansion. Differences in phenotypic

bioRxiv preprint doi: https://doi.org/10.1101/2020.06.30.179952; this version posted July 2, 2020. The copyright holder for this preprint (which was not certified by peer review) is the author/funder, who has granted bioRxiv a license to display the preprint in perpetuity. It is made available under aCC-BY-NC-ND 4.0 International license.

severity likely reflect a role for other *Pu.1*-dependent immune cells, in addition to macrophages, and/or adverse effects resulting from the disruption of cardiac (embryo proper) seeding by primitive macrophages at early stages of embryonic development. Moreover, it is worth mentioning that the genetic ablation approach used here does not discriminate between *bona fide* tissue-resident macrophage and *Csf1r*$^{+}$ EMPs with LEC potential (Fig. 2; (Klotz et al., 2015)). To circumvent this limitation and categorically define a requirement for yolk sac-derived, tissue-resident macrophages, we analyzed the growth of cardiac lymphatics in mice expressing the DTA under the control of *Cx3cr1-CreER* pulsed with tamoxifen at E12.5 (henceforth, *Cx3cr1-CreER;R26R-DTA*). In this model tamoxifen administration of E12.5 leads to selective targeting of yolk sac-derived macrophages, since CX3CR1 is not expressed in fetal liver-derived monocytes or their precursors (Yona et al., 2013). At E16.5, hearts isolated from *Cx3cr1-CreER*$^{+}$ embryos pulsed with tamoxifen at E12.5 exhibited comparatively less LYVE1^{+} tissue-resident macrophages in the subepicardial layer, compared to control littermate samples (Fig. 6A-H), and consequently lymphatic vessel growth was found to be disrupted, with vessel length and number of junctions (i.e. vessel branchpoints) significantly reduced (vessel length: 20866 ± 1088 μm vs. 17800 ± 734.8 μm; $p < 0.05$; number of junctions: 240.9 ± 26.02 vs. 168.0 ± 5.542; $p < 0.05$; Fig. 6I,J), akin to *Csf1r-CreER;R26R-DTA* mutant hearts. This phenotype whilst significant was milder than that observed in *Pu.1*-null hearts, which may be explained by the concomitant replacement of yolk sac-derived macrophages by definitive HSC-derived, blood-borne monocyte progenitors throughout the time-course of lymphatic vessel development (Fig. 2I-L) following ablation of the *Cx3cr1*$^{+}$ lineage. This compensation by further seeding of tissue-resident macrophages is not a factor in *Pu.1*-mutants which lack the entire myeloid lineage (compare Fig. 3F,H,P,R devoid of any resident macrophages in *Pu.1*-null hearts with Fig. 6F,H where there is evidence of residual or replenished LYVE-1+ macrophages in *Csf1r-CreER;R26R-DTA*

bioRxiv preprint doi: https://doi.org/10.1101/2020.06.30.179952; this version posted July 2, 2020. The copyright holder for this preprint (which was not certified by peer review) is the author/funder, who has granted bioRxiv a license to display the preprint in perpetuity. It is made available under aCC-BY-NC-ND 4.0 International license.

mutant hearts). Interestingly, genetic deletion of the *Cx3cr1*$^{+}$ lineage also recapitulated the mis-patterning of the main coronary veins observed in *Csf1r-CreER;R26R-DTA* and *Pu.1*$^{-/-}$ hearts (Fig. 6K-T; white asterisk in O). Collectively these data suggest a hitherto unidentified function for tissue-resident macrophages in regulating the growth, patterning and expansion of the contiguous cardiac lymphatic system.

Macrophage hyaluronan promotes lymphatic cell network formation and sprouting

The close proximity of tissue-resident macrophages to the developing cardiac lymphatics and evident association with the forming lymphatic endothelium, suggests their role in regulating growth and patterning is most likely mediated by cell-cell contact at the leading edges of fusing branches or the adventitial surface of vessel walls (Figs 1-6). To further explore this possibility, we modeled LEC-macrophage interactions during lymphatic capillary tube formation and sprouting in a human *in vitro* setting, by co-culturing human primary lymphatic endothelial cells and human induced pluripotent stem cell (hiPSC)-derived macrophages-labeled with a red fluorescent protein (RFP) reporter (Fig. 7; Movie S1). The hiPSC-derived RFP^{+} macrophages used here have been previously characterized and shown to exhibit fetal-like properties, mimicking the expression profile and function/activity of tissue-resident macrophages (Buchrieser et al., 2017; Haenseler et al., 2017; van Wilgenburg et al., 2013). In tube formation assays, hiPSC-RFP+ macrophages were found in close proximity to, and associated with LECs, changing cell shape to guide LEC extension and fusion to a neighboring LEC, leading to vessel-like structures (Fig. 7A-F; white arrowheads), analogous to the behavior we observed for embryonic macrophages in the developing heart (Fig. 1). Time-lapse live imaging revealed this to be a highly dynamic process, with individual RFP-labelled cells uncoupling from an individual LEC once a tube was formed and scanning the neighboring micro-environment for further LECs undergoing an equivalent

bioRxiv preprint doi: https://doi.org/10.1101/2020.06.30.179952; this version posted July 2, 2020. The copyright holder for this preprint (which was not certified by peer review) is the author/funder, who has granted bioRxiv a license to display the preprint in perpetuity. It is made available under aCC-BY-NC-ND 4.0 International license.

transformation (Movie S1). Likewise, coincident with most of the tube-like structures becoming organized into a plexus, hiPSC-macrophages expressing CD68 were found directly associated with the forming tubes and branching nodes (Fig. 7G-K), phenocopying the behavior observed *in vivo* for tissue-resident embryonic macrophages interacting with cardiac lymphatics (e.g. Fig. 1Q). To model lymphatic sprouting, as an essential first step in lymphatic growth and patterning, we employed two independent three-dimensional (3D) assays based on co-culturing primary human LEC-coated micro-beads (hereafter referred to as the Beads assay) or aggregates of human LECs (the Spheroids assay) with iPSC-derived macrophages (Fig. 7L-X)(Schulz et al., 2012). In the former assay, co-culturing LEC-coated micro-beads with macrophages led to a significant increase in the number of lymphatic-like sprouts per micro-bead, compared to control culture conditions with macrophage:LEC media alone, with RFP-expressing macrophages adjoining and in direct contact with the sprout-leading LEC (control conditions, 100% vs. +macrophages, 173.7 ± 12.90% sprouting activity; $p < 0.001$; Fig. 7L-P). A similar increase in lymphatic sprouting was observed in the spheroids assay (control conditions, 100% vs. +macrophages, 130.9 ± 9.387% sprouting activity; $p < 0.01$; Fig. 7Q-X). To gain insight into the molecular mechanism(s) underpinning stimulation of LEC sprouting by macrophages, we considered paracrine secretion of VEGF-C, a potent lymphangiogenic factor known to be expressed by cardiac macrophages in a myocardial infarction setting (Vieira et al., 2018), and cell adhesion molecules previously implicated in leukocyte-endothelium interactions during immune response, specifically integrin subunit β2 (ITGB2; also known as CD18)- and hyaluronan (HA)-dependent pathways (Gahmberg, 1997; Jackson, 2019; Johnson et al., 2017). Whilst *VEGFC* expression was undetectable, iPS-derived macrophages expressed both *ITGB2* and *ITGAM* (also known as CD11b), the heterodimeric components of the essential macrophage antigen-1 (MAC-1) receptor that binds to endothelial intracellular adhesion molecule-1

bioRxiv preprint doi: https://doi.org/10.1101/2020.06.30.179952; this version posted July 2, 2020. The copyright holder for this preprint (which was not certified by peer review) is the author/funder, who has granted bioRxiv a license to display the preprint in perpetuity. It is made available under aCC-BY-NC-ND 4.0 International license.

(ICAM-1) during leukocyte arrest, rolling and transmigration across the blood vessel wall (Gahmberg, 1997). Notably, they also exhibited a dense coat of HA (previously termed the HA glycocalyx (Johnson et al., 2017; Lawrance et al., 2016)) and expressed the HA-binding receptors *LYVE-1*, *CD44* and *HMMR* (hyaluronan-mediated motility receptor; also known as CD168) (Fig. S3A-D). To discriminate between potential HA and CD18-mediated adhesion to endothelium, we pre-treated iPSC-derived macrophages with hyaluronidase (HAase) to deplete surface glycocalyx-associated HA (Johnson et al., 2017; Lawrance et al., 2016), or with siRNA oligonucleotides targeting *ITGB2/CD18* to specifically knockdown expression of this β integrin subunit without effecting that of the related *ITGAM* expression (Figures S3B-F). We found that loss of macrophage *ITGB2/CD18* had no effect on sprouting activity, but macrophage pre-treatment with HAase significantly impaired LEC sprouting in both bead and spheroid sprouting assays (beads assay: +macrophages, 173.7 ± 12.90 vs. HAase, 96.90 ± 7.205% sprouting activity; $p < 0.001$; spheroids assay: +macrophages, 130.9 ± 9.387 vs. HAase, 80.11 ± 5.588% sprouting activity; $p < 0.001$; Fig. 7O-X), indicating a requirement for macrophage hyaluronan in human lymphatic endothelial growth. Importantly, yolk sac-derived macrophages residing in the HA-rich layer of the epicardium/subepicardium compartment of the developing mouse heart were also found to lack VEGF-C expression and displayed membrane-bound HA (Fig. S4). Taken together with our *Pu.1*$^{-/-}$, *Csf1r-CreER;R26R-DTA* and *Cx3cr1-CreER;R26R-DTA* mutant analyses (Figs 3,5,6), these findings suggest a critical requirement for an evolutionarily-conserved (mouse to human) HA-dependent mechanism underpinning direct cell-cell contact/adhesion between macrophages and LECs during vessel extension and remodeling.

bioRxiv preprint doi: https://doi.org/10.1101/2020.06.30.179952; this version posted July 2, 2020. The copyright holder for this preprint (which was not certified by peer review) is the author/funder, who has granted bioRxiv a license to display the preprint in perpetuity. It is made available under aCC-BY-NC-ND 4.0 International license.

Discussion

Here, we have revealed a novel function for macrophages residing in the developing heart as lymphatic vessel "remodelers" (Figs 1-7). Our findings indicate that primitive macrophages migrate from the yolk sac to the developing heart between E9.25 to E10.5 to initially colonize the outer surface of the ventricular wall, where they reside in the epicardium/subepicardium compartment prior to cardiac lymphatic vessel formation. This compartment has previously been suggested as an essential signaling axis, with epicardial disruption downstream of Wilms' tumor 1 (*Wt1*) gene deficiency impairing cardiac recruitment of yolk sac macrophages (Stevens et al., 2016). However, the identity of the epicardial signal(s) required for this process has remained elusive. Our scRNA-seq analysis of E10.5 hearts (Fig. S1) revealed that expression of the cytokine *Csf1* was exclusively expressed in epicardial cells. CSF1 regulates the differentiation of most macrophage populations, including primitive yolk sac-derived, and is a potent macrophage-chemoattractant (Ginhoux et al., 2010) and, therefore, is a likely mediator of macrophage recruitment into the subepicardial region of the developing heart. Future studies investigating the control of *Csf1* activity by epicardial factors such as WT1 should provide insight into the molecular basis leading to cardiac seeding by yolk sac-derived macrophages.

The epicardium plays an essential role during heart development by secreting paracrine signals stimulating cardiomyocyte proliferation and maturation, as well as supporting cardiac vasculature expansion (Simoes & Riley, 2018). Within the subepicardial space, tissue-resident macrophages co-exist with both coronary and lymphatic endothelium. Our study attributes novel function to these resident macrophages in regulating cardiac lymphatic growth and patterning, along the base-apex axis and laterally to cover both dorsal and ventral surfaces of the developing heart. Tissue-resident macrophages were observed proximal and in

bioRxiv preprint doi: https://doi.org/10.1101/2020.06.30.179952; this version posted July 2, 2020. The copyright holder for this preprint (which was not certified by peer review) is the author/funder, who has granted bioRxiv a license to display the preprint in perpetuity. It is made available under aCC-BY-NC-ND 4.0 International license.

443 direct contact with lymphatic vessels, where they accumulated at branch points. Moreover, in
444 three independent mutant mouse models, *Pu.1*$^{-/-}$, *Csf1r-CreER;R26R-DTA* and *Cx3cr1-*
445 *CreER;R26R-DTA*, macrophage depletion resulted in a truncated and mis-patterned
446 lymphatic plexus, suggesting an essential role in modulating the extension and branching of
447 the lymphatic endothelium (Figs 3,5,6).
448
449 A previous study reported an analogous role for embryonic macrophages in the remodeling of
450 the primitive coronary blood plexus (Leid et al., 2016). Here the authors reported that
451 resident macrophages control the selective expansion of perfused blood vessels, and that an
452 absence of macrophages resulted in hyper-branching of the developing coronaries (Leid et
453 al., 2016). In contrast, we observed a transient reduction in vessel growth and branching (Fig.
454 4), and a mild, but reproducible mis-patterning of the coronary vessels following macrophage
455 depletion in *Pu.1*$^{-/-}$, *Csf1r-CreER;R26R-DTA* and *Cx3cr1-CreER;R26R-DTA* mutant mice
456 (Figs. 4-6). Our findings are supported by studies documenting reduced vessel branching in
457 alternative vascular beds of mice lacking embryonic macrophages, such as the developing
458 hindbrain and postnatal retina (Fantin et al., 2010). Thus, the differences in severity of
459 phenotype between our analyses and that of Leid and colleagues could be due to distinct
460 mouse models used and/or approaches employed to characterize the coronary vasculature
461 (whole-mount heart immunostaining in this study, versus analyses of cryosections in the
462 previous (Leid et al., 2016)).
463
464 At a molecular level, the remodeling of the lymphatic vasculature could arise from
465 macrophage phagocytic activity, release of soluble cytokines or cell-cell interactions. Tissue-
466 resident macrophages have been reported to control various processes during vessel
467 development, in a variety of blood and lymphatic vascular beds, mediated by secretion of

bioRxiv preprint doi: https://doi.org/10.1101/2020.06.30.179952; this version posted July 2, 2020. The copyright holder for this preprint (which was not certified by peer review) is the author/funder, who has granted bioRxiv a license to display the preprint in perpetuity. It is made available under aCC-BY-NC-ND 4.0 International license.

trophic factors. These include, regression of the transient hyaloid endothelium by inducing WNT7B-driven cell death (Lobov et al., 2005), inhibition of branch formation in the developing lymphatic system in the diaphragm through secretion of an elusive factor (Ochsenbein et al., 2016), controlling LEC proliferation in dermal lymphatics (Gordon et al., 2010), mediating coronary blood plexus remodeling through selective expansion of the perfused vasculature *via* putative insulin-like growth factor (IGF) signaling (Leid et al., 2016). In contrast, our findings in the developing mouse heart and *in vitro* models of human lymphatic capillary tube formation and sprouting (Figs 3,5-7) favor a mechanism mediated by direct macrophage-endothelial cell physical contact/adhesion (Fig.1), similar to the role of macrophages in the developing hindbrain and retina vasculature (Fantin et al., 2010). In particular, a requirement for macrophage HA in lymphatic sprouting was identified (Fig. 7). HA is a key structural component of the vertebrate extracellular matrix and has recently been implicated in the postnatal development and response to adult injury (inflammation-driven) of murine corneal lymphangiogenesis (Sun et al., 2019), a process that also depends on the presence of macrophages (Maruyama et al., 2012). Hyaluronan levels are determined, partly by three hyaluronan synthases (HAS1-3), and three hyaluronidases (HYAL1-3) (Triggs-Raine & Natowicz, 2015). HA is also known to interact with different cell surface receptors, including LYVE-1, CD44 and HMMR/CD168 to directly influence endothelial cell motility, proliferation and survival, though the role of such receptors in the regulation of hyaluronan levels remains elusive (Savani et al., 2001; Triggs-Raine & Natowicz, 2015). As such, functional redundancy by different HA binding proteins likely contributes to the lack of a developmental (lymphatic) phenotype in *Lyve1* and *Cd44* single and compound knockout mice (Gale et al., 2007; Luong et al., 2009). Conversely, genetic disruption of hyaluronan synthesis abrogated normal cardiac morphogenesis leading to mid-gestation demise of mutant embryos and impaired the response of cardiac macrophages to ischemia reperfusion injury

bioRxiv preprint doi: https://doi.org/10.1101/2020.06.30.179952; this version posted July 2, 2020. The copyright holder for this preprint (which was not certified by peer review) is the author/funder, who has granted bioRxiv a license to display the preprint in perpetuity. It is made available under aCC-BY-NC-ND 4.0 International license.

493 resulting in poor macrophage survival and functional cardiac output (Camenisch et al., 2000;
494 Petz et al., 2019). Thus, further studies are needed to dissect out the HA/HA-binding receptor
495 axis required for macrophage-induced lymphatic sprouting. Likewise, an indirect effect, *via*
496 the release of a soluble growth factor(s) by tissue-resident macrophages cannot be
497 categorically ruled out at this stage, albeit we can discount VEGF-C given the lack of
498 expression by macrophages in the developing heart (Fig. S4).
499
500 We assign a novel function to the yolk sac-derived, tissue-resident macrophage lineage,
501 against a back-drop of a rapidly evolving field which attributes ever increasing plasticity, in
502 terms of cell fate and signaling, to these essential resident lineages. This is complemented by
503 insights into our fundamental understanding as to how discrete organ-based vascular beds are
504 formed and the degree of heterogeneity in terms of cellular contributions to organ-specific
505 endothelium. Live imaging in the adult mouse and zebrafish recently demonstrated that
506 inflammatory macrophages are required for orchestration of skin wound neoangiogenesis
507 (Gurevich et al., 2018). Likewise, macrophages of diverse phenotypes supported
508 vascularization of 3D human engineered tissues (Graney et al., 2020). Moreover, the
509 maintenance of the mouse choroidal vascular network, as well as lymphatic vessels in the
510 cornea is dependent on the presence of macrophages, with decreased macrophage number
511 and activation leading to reduced lymphatic vessel formation and contributing to impaired
512 diabetic wound healing in a mouse model of corneal wound healing (Maruyama et al., 2007;
513 Maruyama et al., 2012; Yang et al., 2020). Importantly the close interaction between cardiac
514 lymphatics and macrophages during development, appears to manifest in the postnatal heart
515 via infiltrating inflammatory macrophages and injury-activated lymphangiogenesis following
516 myocardial infarction (Klotz et al., 2015; Vieira et al., 2018). The functional role for
517 macrophages in directly regulating lymphatic growth and remodeling during development we

bioRxiv preprint doi: https://doi.org/10.1101/2020.06.30.179952; this version posted July 2, 2020. The copyright holder for this preprint (which was not certified by peer review) is the author/funder, who has granted bioRxiv a license to display the preprint in perpetuity. It is made available under aCC-BY-NC-ND 4.0 International license.

518 report herein may, therefore, manifest in response to injury in the adult setting. Taken
519 together, this further strengthens the rationale for extrapolating from our developmental
520 studies to therapeutically target macrophage-lymphatic responses during postnatal
521 cardiovascular disease/injury.

bioRxiv preprint doi: https://doi.org/10.1101/2020.06.30.179952; this version posted July 2, 2020. The copyright holder for this preprint (which was not certified by peer review) is the author/funder, who has granted bioRxiv a license to display the preprint in perpetuity. It is made available under aCC-BY-NC-ND 4.0 International license.

MATERIAL AND METHODS

Key resources table

REAGENT or RESOURCE	SOURCE	IDENTIFIER
Antibodies		
Rat monoclonal anti-mouse EMCN (clone V.5C7)	Santa Cruz Biotech (1:50)	Cat# sc-53941
Rabbit polyclonal anti-mouse LYVE-1	AngioBio (1:100)	Cat# 11-034
Armenian Hamster monoclonal anti-mouse PECAM-1/CD31 (clone 2H8)	Abcam (1:100)	Cat# ab119341
Rat monoclonal anti-mouse LYVE-1 (clone ALY7)	Novus Biologicals (1:100)	Cat# NBP1-43411
Goat polyclonal anti-mouse VEGFR3/Flt4	R&D (1:100)	Cat# AF743
Goat polyclonal anti-human PROX1	R&D (1:100)	Cat# AF2727
Chicken polyclonal anti-GFP	Abcam (1:200)	Cat# ab13970
Rat monoclonal anti-mouse CD68 (clone FA-11)	Bio-Rad (1:100)	Cat# MCA1957
Rabbit anti-VEGF-C	Abcam (1:100)	Cat# ab9546
Alexa Fluor 647 Rat anti-mouse CD45 (clone 30-F11)	Biolegend (1:100)	Cat# 103124
FITC Rat anti-mouse CD11b (clone M1/70)	Biolegend (1:100)	Cat# 101206
PE Rat anti-mouse F4/80 (clone BM8)	Biolegend (1:100)	Cat# 123110
Rabbit polyclonal anti-mouse p-Histone H3 (Ser10)	Santa Cruz Biotech (1:100)	Cat# sc-8656-R
Rat polyclonal anti-mouse CD31 (clone MEC13.3)	BD Pharmingen (1:100)	Cat# 550274
Mouse monoclonal Anti-human CD68 (clone KP1)	Abcam (1:100)	Cat# 955
Alexa Fluor 568 Phalloidin	Invitrogen (1:100)	Cat# A12380
Chemicals, Peptides, and Recombinant Proteins		
Paraformaldehyde (PFA) solution 4% in PBS	Santa Cruz Biotech	Cat# 281692
Cytodex 3 microcarrier beads	Sigma-Aldrich	Cat# C3275
7-amino-actinomycin D (7-ADD)	BD Pharmingen	Cat# 559925
DAPI solution	Invitrogen	Cat# 62248
EGM-2MV medium	PromoCell	Cat# C-22022
EGM2-Incomplete medium (EGM2 medium not supplemented with FGF, VEGF-A and EGF)	Lonza	Cat# CC-3162
Red Blood Cell lysis buffer (10x)	Biolegend	Cat# 420301
Collagenase, Type II	Worthington	Cat# LS004180
CellTracker Green CMFDA Dye	Invitrogen	Cat# C2925
Human Type 1 Atelo-Collagen solution, 1 mg/ml	Advanced Bio-matrix	Cat# 5007-20ML
D-erythro-sphingosine-1-phosphate (d18:1)	Avanti Polar Lipids	Cat# 860492P
Experimental Models: Cell Lines		
Human: Primary dermal lymphatic endothelial cells (HDLEC)	PromoCell	Cat# C-12216
Human: iPS-derived macrophages-RFP	James Martin Stem Cell Facility-University of Oxford	Haenseler W et al. (2017) *Stem cell Reports* 8:1727.

bioRxiv preprint doi: https://doi.org/10.1101/2020.06.30.179952; this version posted July 2, 2020. The copyright holder for this preprint (which was not certified by peer review) is the author/funder, who has granted bioRxiv a license to display the preprint in perpetuity. It is made available under aCC-BY-NC-ND 4.0 International license.

Experimental Models: Organisms/Strains		
Mouse: *Cx3cr1-GFP: B6.129P2(Cg)-Cx3cr1^{tm1Litt}/J*	The Jackson Laboratory	JAX: 005582
Mouse: *Cx3cr1-CreER: B6.129P2(Cg)-Cx3cr1$^{tm2.1(cre/ERT2)Litt}$/WganJ*	The Jackson Laboratory	JAX: 021160
Mouse: *Csf1r-CreER: FVB-Tg(Csf1r-cre/Esr1*)1Jwp/J*	The Jackson Laboratory	JAX: 019098
Mouse: *R26R-DTA: Gt(ROSA)26Sor$^{tm1(DTA)Jpmb}$/J*	The Jackson Laboratory	JAX: 006331
Mouse: *R26R-tdTomato: B6;129S6-Gt(ROSA)26Sor$^{tm14(CAG-tdTomato)Hze}$/J*	The Jackson Laboratory	JAX: 007908
Mouse: *Flt3-CreERT2*	Sten Eirik Jacobsen's laboratory, Karolinska Institutet, Sweden	Benz et al. (2008) *J. Exp. Medicine* 205: 1187.
Mouse: *hCD68-GFP*	David R. Greaves' laboratory, University of Oxford, UK	Iqbal et al. (2014) *Blood* 124: e33
Mouse: *Pu.1-/-*	Paul Martin's laboratory, University of Bristol, UK	McKercher et al. (1996) *EMBO J.* 15: 5647.
Software and Algorithms		
Fiji-Image J	NIH	N/A
Photoshop	Adobe	N/A
Zen	Zeiss	N/A
Prism 8	GraphPad	N/A
AngioTool	Zudaire et al. (2011) *PLoS One* 6:e27385	N/A
FlowJo	LLC	N/A

Mouse lines

Genetically modified mouse lines used in the study were kept in a pure C57BL/6 genetic background and are listed in **Key resources table**. *Cx3cr1-GFP* knock-in mice and *hCD68-GFP* transgenic mice were crossed with C57BL/6 to generate *Cx3cr1$^{GFP/+}$* and *hCD68-GFP^{+}* samples, respectively. *Pu.1$^{+/-}$* mice were intercrossed to generate *Pu.1$^{-/-}$* specimens. *Csf1r-CreER* transgenic mice, *Cx3cr1-CreER* knock-in mice and *Flt3-CreERT2* transgenic mice were crossed with *R26R-tdTomato* or *R26R-DTA* reporters strains to generate *Csf1r-CreER;tdTomato, Csf1r-CreER;R26R-DTA, Cx3cr1-CreER;R26R-tdTomato, Cx3cr1-*

bioRxiv preprint doi: https://doi.org/10.1101/2020.06.30.179952; this version posted July 2, 2020. The copyright holder for this preprint (which was not certified by peer review) is the author/funder, who has granted bioRxiv a license to display the preprint in perpetuity. It is made available under aCC-BY-NC-ND 4.0 International license.

CreER;R26R-DTA and *Flt3-CreERT2;tdTomato* mice. *Pu.1*$^{-/-}$*;Csf1r-CreER;tdTomato* compound transgenic mice were generated by crossing *Pu.1*$^{+/-}$*;Csf1r-CreER* with *Pu.1*$^{+/-}$*;R26R-tdTomato* mice. Both males and females were used in the study. For timed-mating experiments, 8-16-week-old mice were set up overnight and females checked for vaginal plugs the following morning; the date of a vaginal plug was set as embryonic day (E) 0.5. For tamoxifen-dependent tissue-specific gene activation, 75mg/Kg/dose of tamoxifen (Sigma) were administered to pregnant dams, intraperitoneally (i.p.). Mice were housed and maintained in a controlled environment by the University of Oxford Biomedical Services. All animal experiments were carried out according to the UK Home Office project license (PPL) 30/3155 and PPDE89C84 compliant with the UK animals (Scientific Procedures) Act 1986 and approved by the local Biological Services Ethical Review Process.

Cell lines

Primary human dermal lymphatic endothelial cells (HDLEC) isolated from the dermis of juvenile foreskin (PromoCell) were cultured in presence of endothelial cell growth medium (ECGM)-MV2 (PromoCell), according to the manufacturer' instructions. Human iPS-derived macrophages constitutively expressing RFP (Haenseler et al., 2017) were obtained from the James Martin Stem Cell Facility (Sir William Dunn School of Pathology, University of Oxford, UK). The human iPS cell line was derived previously from dermal fibroblasts of a healthy donor that had given signed informed consent for the derivation of iPS cells (Ethics Committee: National Health Service, Health Research Authority, NRES Committee South Central, Berkshire, UK (REC 10/H0505/71)). iPS-macrophages were cultured in macrophage medium composed of X-VIVO™15 (Lonza), GlutaMax (Invitrogen) and M-CSF (Invitrogen), as previously described (van Wilgenburg et al., 2013). Cell lines were maintained in a humidified atmosphere of 5% CO_2 at 37^{o}C.

bioRxiv preprint doi: https://doi.org/10.1101/2020.06.30.179952; this version posted July 2, 2020. The copyright holder for this preprint (which was not certified by peer review) is the author/funder, who has granted bioRxiv a license to display the preprint in perpetuity. It is made available under aCC-BY-NC-ND 4.0 International license.

Sample preparation for immunostaining

Embryos were harvested at the required embryonic stage, placed in ice-cold PBS (Sigma) and the amniotic sac was removed. The heart was micro-dissected from the embryo for immunostaining experiments using fine forceps. Dissected hearts were fixed for 6 hours in 2% PFA/PBS at room temperature, permeabilized in 0.3% Triton X-100/PBS (twice, 10 minutes each) and then blocked in 1% BSA, 0.3% Triton X-100 in PBS for at least 2 hours. Samples from fluorescent reporter lines (e.g. *Cx3cr1-GFP* and *CD68-GFP*) were protected from light throughout this procedure. Samples were incubated with primary antibodies (diluted in block; listed in **Key resources table**) overnight at 4°C, then washed three times for at least 1 hour each in 0.3% Triton X-100/PBS. Samples were incubated with Alexa Fluor®-conjugated secondary antibodies (diluted in PBS; Invitrogen) overnight at 4°C, protected from light, then rinsed three times for at least 10 minutes each with PBS. The hearts were then orientated according to dorsal-ventral surface aspect and mounted in 50% glycerol/PBS in glass-bottomed dishes (Mattek). Imaging was performed using an Olympus FV 1000 or Zeiss LSM 780 scanning confocal microscope. Images were digitally captured and processed using Zen and FIJI-Image J software. Analysis of total vessel length and junction number calculation were performed using AngioTool software (Zudaire et al., 2011).

Preparation of single cell suspensions from the heart

Fetal hearts harvested for flow cytometry studies were isolated, placed in ice-cold HBSS (Life Technologies), finely minced into small pieces, and digested with collagenase type II (Worthington Laboratories) solution (containing 500units/ml HBSS) at 37°C for 30 minutes with agitation at 180 rpm. Dissociated samples were then passed into a 50-mL conical tube (Corning) through a 70-μm cell strainer, then rinsed with 3 mL ice-cold HBSS and

bioRxiv preprint doi: https://doi.org/10.1101/2020.06.30.179952; this version posted July 2, 2020. The copyright holder for this preprint (which was not certified by peer review) is the author/funder, who has granted bioRxiv a license to display the preprint in perpetuity. It is made available under aCC-BY-NC-ND 4.0 International license.

583 transferred back to a 15-mL conical tube. Samples were spun for 7 minutes at 350 *g* at 4°C,
584 and the supernatant carefully discarded. Cell pellets were resuspended in 5 mL of Red Blood
585 Cell (RBC) lysis buffer (BioLegend) and incubated at room temperature for 10 minutes,
586 followed by a repeat centrifugation at 350 *g* at 4°C for 7 minutes. The RBC lysis buffer was
587 removed, and cells resuspended in 2% FBS/PBS. Isolated single cardiac cells were stained
588 and subjected to flow cytometry analyses.
589
590 **Flow cytometry**
591 Using 7-AAD exclusion (BD Pharmingen), only live cells were analysed. All antibodies used
592 for flow cytometry are listed in **Key resources table**. Flow cytometric analyses were
593 performed using FACSAria III flow cytometer (BD Biosciences) and FlowJo software
594 (LLC). Samples resuspended in 2% FBS/PBS solution were blocked with mouse Fc Block
595 (Miltenyi Biotec) for 5 minutes on ice, followed by labelling for 20 minutes at room
596 temperature with each antibody combination.
597
598 **Time-lapse tube formation assay**
599 384-well plates (PerkinElmer) were coated with Growth Factor-reduced Matrigel (Corning)
600 and incubated for 30 minutes at 37°C. 25 µL of ECGM-MV2 containing 4,500 HDLECs
601 were added per well and incubated for 60 minutes at 37°C. Then, 25 µL of macrophage
602 media containing 2,250 human iPS-derived macrophages-RFP were added per well. For time-
603 lapse imaging acquisition, an Evos® FL Auto Cell Imaging System (ThermoFisher) was used
604 and one image was taken every 8 minutes for 15 hours. At the end of image acquisition, cells
605 were fixed with 4% PFA solution (Santa Cruz Biotech) for 30 min and washed with PBS for
606 further analysis (e.g. immunostaining).
607

bioRxiv preprint doi: https://doi.org/10.1101/2020.06.30.179952; this version posted July 2, 2020. The copyright holder for this preprint (which was not certified by peer review) is the author/funder, who has granted bioRxiv a license to display the preprint in perpetuity. It is made available under aCC-BY-NC-ND 4.0 International license.

Immunostaining of HDLEC-macrophage co-cultures

HDLEC-like tubes were permeabilized with 0.1% Triton X-100/PBS and then incubated with a staining solution containing Alexa Fluor® 568 Phalloidin and DAPI (both Invitrogen). Immunofluorescence staining was performed using an antibody against human CD68 (Abcam).

iPS-derived macrophage transfection

Macrophages were transfected in a 24-well plate as previously described (Troegeler et al., 2014). Macrophages were washed twice with warm complete XVIVO in order to remove floating cells. 250 µL of fresh complete XVIVO were added per well and cells kept at 37□C and 5% CO2. 3,75 uL of siRNA (20 uM - Thermofisher), 110.25 uL XVIVO depleted (without MCSF) and 11 uL HiPerfect (Qiagen) were gently mixed in a tube and incubated at room temperature for 15 to 20 min. 125 uL of the mix was then added in each well drop by drop. The plate was gently rocked to assure nice distribution of the mix. After 6 hours, 0.5 mL of Complete XVIVO was added and the cells were harvested 3 days later for RNA extraction and/or experimental procedures.

HAase treatment and immunostaining

Macrophages were seeded on coverslips and treated with 15 U/mL or 30 U/mL hyaluronidase (HAase - Sigma) 2 hours prior experiment. For staining, cells were fixed with 4% PFA and permeabilized in 0.2% Triton X-100/PBS for 10 min and then blocked in 1% BSA, 0.1% Triton X-100 in PBS for at least 2 hours. Macrophages were incubated with 3 ug/mL biotinylated Hyaluronan binding protein (Amsbio) overnight at 4°C, then washed three times with PBS. Samples were incubated with Alexa Fluor® 488 Streptavidin (diluted in PBS; Biolegend) overnight at 4°C, protected from light, then rinsed three times for at least 10

bioRxiv preprint doi: https://doi.org/10.1101/2020.06.30.179952; this version posted July 2, 2020. The copyright holder for this preprint (which was not certified by peer review) is the author/funder, who has granted bioRxiv a license to display the preprint in perpetuity. It is made available under aCC-BY-NC-ND 4.0 International license.

minutes each with PBS. Coverslip were then mounted on slides using Vectashield + DAPI (Vector Laboratories).

Microbeads capillary sprouting assay

The capillary sprouting assay was performed as previously described (Schulz et al., 2012). HDLECs were incubated in a 15-mL conical tube in presence of cytodex 3 beads (Sigma) at a ratio of 400 cells per bead in EGM-2MV medium (Lonza) for 4 hours at 37°C with shaking every 20 minutes. Beads were then incubated in a cell flask at 37°C for 48 hours in EGM-2MV medium. The HDLEC-coated beads were subsequently collected and labelled with 2 µM Cell Tracker Green dye (Invitrogen) for 30 minutes, embedded in 1mg/mL Type I collagen hydrogel (Advanced Bio-Matrix), containing 2 µM D-erythro-sphingosine-1-phosphate (Avanti Polar Lipids), and cultured in black clear-bottom 96-well plates (Perkin-Elmer) in the presence or absence of 10,000 human iPS-derived macrophages-RFP per well. After 60 minutes of incubation, a 1:1 mix containing EGM2-Incomplete (EGM2 media without supplementation with EGF, FGF2 and VEGF-A; Lonza) and macrophage media (v/v) was added and the beads incubated for two days at 37°C. Then, the beads were fixed with 4% PFA for 30 minutes and washed twice with PBS. Each well was imaged with a Zeiss LSM 780 scanning confocal microscope and the number of sprouts per bead calculated.

Spheroids sprouting assay

Spheroids of 400 HDLECs were generated using a 24-well plate Aggrewell 400 (Stemcells Technologies) using EGM2-Incomplete. The following day, spheroids were collected and embedded in 1mg/mL Type I collagen hydrogel and cultured in black clear-bottom 384-well plates (Perkin-Elmer) in the presence or absence of 2,5k human iPS-derived macrophages-RFP per well. After 60 minutes of incubation, a 1:1 mix containing EGM2-Incomplete

bioRxiv preprint doi: https://doi.org/10.1101/2020.06.30.179952; this version posted July 2, 2020. The copyright holder for this preprint (which was not certified by peer review) is the author/funder, who has granted bioRxiv a license to display the preprint in perpetuity. It is made available under aCC-BY-NC-ND 4.0 International license.

(Lonza) and macrophage media (v/v) was added and the spheroids incubated for two days at 37°C. Then, the spheroids were fixed with 2% PFA for 30 minutes, washed twice with PBS and stained with Alexa Fluor® 488 phalloidin (Invitrogen). Each well was imaged with an automated cell imaging system (Pico microscope - Molecular device) and the number of sprouts per spheroids calculated.

RNA extraction and qRT-PCR

Total RNA was extracted using Trizol Reagent (Invitrogen). Reverse transcription (RT) was performed using SuperScript(R) III Reverse Transcriptase (Invitrogen), as recommended by the manufacturer. Primer sequences (Invitrogen) used were:

*36B4*_F CTACAACCCTGAAGAAGTGCTTG

*36B4*_R CAATCTGCAGACAGACACTGG

*CSF1R*_F CCTCACTGGACCCTGTACTC

*CSF1R*_R GGAAGGTAGCGTTGTTGGTG

*CX3CR1*_F ACCAACTCTTGCAGGTCTC

*CX3CR1*_R TGTCAGCACCACAACTTGG

*ITGB2/CD18*_F GTCTTCCTGGATCACAACGC

*ITGB2/CD18*_R CAAACGACTGCTCCTGGATG

*ITGAM/CD11b*_F CAGTGAGAAATCCCGCCAAG

*ITGAM/CD11b*_R CCGAAGCTGGTTCTGAATGG

*VEGFC*_F GGAGGCTGGCAACATAACAG

*VEGFC*_R TTTGTCGCGACTCCAAACTC

*LYVE1*_F CTGGGTTGGAGATGGATTCG

*LYVE1*_R TCAGGACACCCACCCCATTT

*CD44*_F AAGTGGACTCAACGGAGAGG

bioRxiv preprint doi: https://doi.org/10.1101/2020.06.30.179952; this version posted July 2, 2020. The copyright holder for this preprint (which was not certified by peer review) is the author/funder, who has granted bioRxiv a license to display the preprint in perpetuity. It is made available under aCC-BY-NC-ND 4.0 International license.

683 *CD44*_R GTCCACATTCTGCAGGTTCC

684 *HMMR/CD168*_F GGCTAAGCAAGAAGGCATGG

685 *HMMR/CD168*_R TCCCTCCAGTTGGGCTATTT

686 Real□time polymerase chain reaction (PCR) assays were run on a ViiA 7 step real□time
687 PCR machine (Applied□Biosystems). Normalization was performed using *36B4* as a
688 reference gene. Quantification was performed using the comparative Ct method.

689

690 **scRNA-seq and analysis**

691 E7.75_E8.25_E9.25 10x Chromium data (GSE126128) were downloaded from UCSC Cell
692 Browser as raw UMI count matrix (de Soysa et al., 2019). Only the E9.25 datasets were
693 selected for further analysis. E10.5 heart 10x Chromium data were downloaded as raw counts
694 from GEO (GSE131181) (Hill et al., 2019). All scRNA-seq datasets were analyzed using
695 Seurat (Butler et al., 2018; Stuart et al., 2019) in R as follows: individual replicates were
696 integrated using SCTransform method, principal component analysis was used to define the
697 cell clusters, which were visualized with the UMAP method (Becht et al., 2018; Butler et al.,
698 2018).

699

700 **Statistical analysis**

701 All data are presented as mean ± standard error of the mean (SEM). Statistical analysis was
702 performed on GraphPad Prism 8 software. The statistical significance between two groups
703 was determined using an unpaired two-tailed Student's *t*-test, these included an F-test to
704 confirm the two groups had equal variances. Among three or more groups (e.g. data shown in
705 Fig. 1A), one-way analysis of variance (ANOVA) followed up by Tukey's multiple
706 comparison test was used for comparisons. A value of $p \leq 0.05$ was considered statistically
707 significant.

bioRxiv preprint doi: https://doi.org/10.1101/2020.06.30.179952; this version posted July 2, 2020. The copyright holder for this preprint (which was not certified by peer review) is the author/funder, who has granted bioRxiv a license to display the preprint in perpetuity. It is made available under aCC-BY-NC-ND 4.0 International license.

Contact for reagent and resource sharing

Further information and requests for resources and reagents should be directed to and will be fulfilled by the Lead Contact, Paul R. Riley (paul.riley@dpag.ox.ac.uk).

bioRxiv preprint doi: https://doi.org/10.1101/2020.06.30.179952; this version posted July 2, 2020. The copyright holder for this preprint (which was not certified by peer review) is the author/funder, who has granted bioRxiv a license to display the preprint in perpetuity. It is made available under aCC-BY-NC-ND 4.0 International license.

712 **Acknowledgements**

713 We would like to thank Paul Martin (School of Biochemistry, University of Bristol, Bristol,
714 UK) for the kind permission to use the *Pu.1*$^{-/-}$ mice on a C57BL/6 genetic background;
715 Micron Oxford Advanced Bioimaging Unit for access to and training in the use of confocal
716 microscopy; and the staff of the University of Oxford Biomedical Services Building for
717 excellent mouse husbandry. We thank the staff at the James Martin Stem Cell Facility, which
718 has received core support from the Oxford Martin School (LC0910-004), Wellcome Trust
719 (WTISSF121302) and MRC (MC EX MR/N50192X/1) for assistance with iPS-macrophage
720 differentiation. This work was funded by the British Heart Foundation (chair award
721 CH/11/1/28798 and programme grant RG/08/003/25264 to PRR) and supported by the BHF
722 Oxbridge Centre of Regenerative Medicine (RM/13/3/30159); a Wellcome Trust Doctoral
723 Training Fellowship 106334/Z/14/Z to TJC; a Wellcome Trust Four year PhD Studentship
724 215103/Z/18/Z to KK; a BHF Intermediate Basic Science Research Fellowship
725 FS/19/31/34158 to JMV; a British Israel Research and Academic Exchange Partnership
726 (BIRAX) Grant 13BX14PRET; a Leducq Foundation Transatlantic Network of Excellence
727 Program 14CVD04 and MRC Unit funding to DGJ.

728

729 **Competing interests**

730 PRR is co-founder and equity holder in OxStem Cardio, an Oxford University spin-out that
731 seeks to exploit therapeutic strategies stimulating endogenous repair in cardiovascular
732 regenerative medicine.

733

734 **Authors Contributions**

735 TJC, XS, JMV and PRR conceived and designed the study. TJC, XS, CVDC and JMV
736 carried out all mouse experiments, including sample generation, immunostaining and

bioRxiv preprint doi: https://doi.org/10.1101/2020.06.30.179952; this version posted July 2, 2020. The copyright holder for this preprint (which was not certified by peer review) is the author/funder, who has granted bioRxiv a license to display the preprint in perpetuity. It is made available under aCC-BY-NC-ND 4.0 International license.

737 imaging. CR performed the macrophage-lymphatic endothelial cell co-culture experiments.
738 TJC performed the flow cytometry studies and analyzed the data generated. IEL performed
739 scRNA-seq analysis and generated UMAP and dot plots. AML and SEWJ generated the *Flt3-*
740 *CreERT2;tdTomato* samples. DRG provided the *hCD68-GFP* reporter mice. DGJ provided
741 significant advice and technical assistance with macrophage-lymphatic cell interactions and
742 involvement of the macrophage hyaluronan surface glycocalyx. CB, SAC and WJ provided
743 iPS-derived macrophages-RFP and technical assistance with co-culture studies. RPC and
744 PRR co-supervised TJC. XS, TJC, CR, KK and JMV analyzed the data. JMV wrote the
745 manuscript. TJC, XS, JMV and PRR edited the manuscript. JMV and PRR supervised the
746 study.
747

bioRxiv preprint doi: https://doi.org/10.1101/2020.06.30.179952; this version posted July 2, 2020. The copyright holder for this preprint (which was not certified by peer review) is the author/funder, who has granted bioRxiv a license to display the preprint in perpetuity. It is made available under aCC-BY-NC-ND 4.0 International license.

FIGURE LEGENDS

Fig. 1. Tissue-resident macrophages are closely associated with the developing cardiac lymphatics. (A) Representative histograms and percentage of tissue-resident macrophages in the developing heart at embryonic days (E)12.5, E14.5 and E16.5 measured by flow cytometry for GFP and F4/80 in *Cx3cr1*$^{GFP/+}$ reporter embryos. GFP^{+}F4/80^{+} are defined as macrophages. Data represent mean ± SEM; n = 6 hearts per group. Significant differences (p values) were calculated using one-way ANOVA followed up by the Tukey's multiple comparison test (*$p \leq 0.05$; **$p \leq 0.01$; ****$p \leq 0.0001$). (B-M) Whole-mount immunostaining for GFP (green), EMCN (red) and LYVE-1 (white) to visualize the sub-epicardial tissue-resident macrophages, coronary vessels (capillaries and veins) and lymphatic plexus (respectively) in both the dorsal and ventral aspects of hearts-derived from *Cx3cr1*$^{GFP/+}$ embryos at E12.5 (B-E), E14.5 (F-I) and E16.5 (J-M). (C,E,G,I,K,M) Magnified views of boxes shown in (B,D,F,H,J,L). Note that LYVE-1 reactivity is detected in the lymphatic endothelium and tissue-resident macrophages. (N-Q) GFP (green) and VEGFR3 (red) immunostaining of whole-mount hearts derived from *CD68-GFP*-expressing embryos at E16.5. (Q) Orthogonal view of the inset box shown in (P); white arrowheads indicate close association of CD68-GFP^{+} macrophages to VEGFR3-expressing lymphatic vessels. (R-U) LYVE-1 (green) and PROX1 (red) immunostaining of whole-mount hearts derived from C57BL6 embryos at E16.5. (U) Orthogonal view of the inset box shown in (T); white arrowheads indicate LYVE-1^{+} macrophages interacting with fusing lymphatic tip cells labelled with PROX1 (nuclear) and LYVE-1 (membrane). All scale bars 100 μm, except in Q 25 μm, R 200 μm and U 50 μm.

bioRxiv preprint doi: https://doi.org/10.1101/2020.06.30.179952; this version posted July 2, 2020. The copyright holder for this preprint (which was not certified by peer review) is the author/funder, who has granted bioRxiv a license to display the preprint in perpetuity. It is made available under aCC-BY-NC-ND 4.0 International license.

Fig. 2. Yolk sac-derived *Csf1r*$^{+}$ and *Cx3cr1*$^{+}$ lineages are associated with cardiac lymphatic growth and expansion. (A-D) Genetic lineage-tracing based on the activity of the *Csf1r-CreER;tdTomato* transgene induced by tamoxifen administration at embryonic day (E)8.5. Whole-hearts were analyzed for Tomato (red) and PROX1 (green) expression at E16.5. (B-D) Magnified views of box shown in (A); white arrowhead indicates co-localization of native Tomato and PROX1 immunoreactivity. (E-H) Genetic lineage-tracing based on the activity of the *Cx3cr1-CreER;tdTomato* transgene induced by tamoxifen administration at E8.5. Whole-hearts were analyzed for Tomato (red) and PROX1 (green) expression at E16.5. (F-H) Magnified views of box shown in (E). (I-L) Genetic lineage-tracing based on the activity of the *Flt3-CreERT2;tdTomato* transgene induced by repeated tamoxifen administration at E13.5 and E15.5. Whole-hearts were analyzed for Tomato (red) and PROX1 (green) expression at E16.5. (J-L) Magnified views of box shown in (I). All scale bars 100 μm.

bioRxiv preprint doi: https://doi.org/10.1101/2020.06.30.179952; this version posted July 2, 2020. The copyright holder for this preprint (which was not certified by peer review) is the author/funder, who has granted bioRxiv a license to display the preprint in perpetuity. It is made available under aCC-BY-NC-ND 4.0 International license.

Fig. 3. Macrophages are essential for growth and branching of the cardiac lymphatic network. (A-H) Whole-mount immunostaining for LYVE-1 (green) to visualize the sub-epicardial lymphatic plexus in both the dorsal and ventral aspects of hearts-derived from littermate control (co; A-D) or *Pu.1*$^{-/-}$ embryos (E-H) at E16.5. (B,D,F,H) Magnified views of inset boxes shown in (A,C,E,G). Note absence of LYVE-1 reactivity in tissue-resident macrophages in *Pu.1*$^{-/-}$ hearts, compared to control littermates, confirming absence of macrophages. (I,J) Quantification of total vessel length (μm; I) and number of lymphatic vessel junctions (J) in Co versus *Pu.1*$^{-/-}$ hearts at E16.5. Data represent mean ± SEM; $n = 6$ hearts per group. Significant differences (p values) were calculated using an unpaired, two-tailed Student's t-test (**$p \leq 0.01$). (K-R) Whole-mount immunostaining for LYVE-1 (green) to visualize the sub-epicardial lymphatic plexus in both the dorsal and ventral aspects of hearts-derived from littermate control (co; K-N) or *Pu.1*$^{-/-}$ embryos (O-R) at E19.5. (L,N,P,R) Magnified views of boxes shown in (K,M,O,Q). (S,T) Quantification of total vessel length (μm; S) and number of lymphatic vessel junctions (T) in Co versus *Pu.1*$^{-/-}$ hearts at E19.5. Data represent mean ± SEM; Co, $n = 5$ hearts; *Pu.1*$^{-/-}$, $n = 6$ hearts. Significant differences (p values) were calculated using an unpaired, two-tailed Student's t-test (*$p \leq 0.05$; ***$p \leq 0.001$). All scale bars 100 μm.

bioRxiv preprint doi: https://doi.org/10.1101/2020.06.30.179952; this version posted July 2, 2020. The copyright holder for this preprint (which was not certified by peer review) is the author/funder, who has granted bioRxiv a license to display the preprint in perpetuity. It is made available under aCC-BY-NC-ND 4.0 International license.

Fig. 4. Macrophages regulate coronary growth and patterning. (A-H) Whole-mount immunostaining for EMCN (red) to visualize the sub-epicardial coronary vessels (capillaries and veins) in both the dorsal and ventral aspects of hearts-derived from littermate control (co; A-D) or *Pu.1*$^{-/-}$ embryos (E-H) at E16.5. (B,D,F,H) Magnified views of boxes shown in (A,C,E,G). White asterisk indicates patterning defects, i.e. an extra mid-branch, of the coronary veins on the dorsal aspect of *Pu.1*$^{-/-}$ hearts (compared E with A). (I,J) Quantification of total vessel length (μm; I) and number of vessel junctions (J) in Co versus *Pu.1*$^{-/-}$ hearts at E16.5. Data represent mean ± SEM; $n = 6$ hearts per group. Significant differences (p values) were calculated using an unpaired, two-tailed Student's t-test (*$p \leq 0.05$; **$p \leq 0.01$). (K-R) Whole-mount immunostaining for EMCN (red) to visualize the sub-epicardial coronary vessels (capillaries and veins) in both the dorsal and ventral aspects of hearts derived from littermate control (co; K-N) or *Pu.1*$^{-/-}$ embryos (O-R) at E19.5. (L,N,P,R) Magnified views of boxes shown in (K,M,O,Q). White asterisks indicate patterning defects, i.e. extra branches, of the coronary veins on both the dorsal and ventral aspects of *Pu.1*$^{-/-}$ hearts (compared O,Q with K,M). (S,T) Quantification of total vessel length (μm; S) and number of vessel junctions (T) in Co versus *Pu.1*$^{-/-}$ hearts at E19.5. Data represent mean ± SEM; Co, $n = 5$ hearts; *Pu.1*$^{-/-}$, $n = 6$ hearts. No significant differences were determined using an unpaired, two-tailed Student's t-test. All scale bars 100 μm, except E 1mm.

bioRxiv preprint doi: https://doi.org/10.1101/2020.06.30.179952; this version posted July 2, 2020. The copyright holder for this preprint (which was not certified by peer review) is the author/funder, who has granted bioRxiv a license to display the preprint in perpetuity. It is made available under aCC-BY-NC-ND 4.0 International license.

Fig. 5. Ablation of the *Csf1r*$^{+}$ lineage impairs cardiac lymphatic growth and branching. (A-H) Whole-mount immunostaining for LYVE-1 (green) to visualize the sub-epicardial lymphatic plexus in both the dorsal and ventral aspects of E16.5 hearts-derived from littermate control (co; A-D) or *Csf1r-CreER;R26R-DTA* embryos (Mut; E-H), tamoxifen-induced at E12.5. (B,D,F,H) Magnified views of boxes shown in (A,C,E,G). (I,J) Quantification of total vessel length (μm; I) and number of lymphatic vessel junctions (J) in Co versus Mut hearts at E16.5. Data represent mean ± SEM; n = 5 hearts per group. Significant differences (p values) were calculated using an unpaired, two-tailed Student's t-test (*$p \leq 0.05$; **$p \leq 0.01$). (K-R) Whole-mount immunostaining for EMCN (red) to visualize the sub-epicardial coronary vessels (capillaries and veins) in both the dorsal and ventral aspects of E16.5 hearts-derived from littermate control (co; K-N) or *Csf1r-CreER;R26R-DTA* embryos (Mut; O-R), tamoxifen-induced at E12.5. (L,N,P,R) Magnified views of boxes shown in (K,M,O,Q). White asterisk indicates patterning defects, i.e. an extra mid-branch, of the coronary veins on the dorsal aspect of *Csf1r-CreER;R26R-DTA* hearts (compared O with K), akin to *Pu.1*-null hearts (compared to Fig. 3). (S,T) Quantification of total vessel length (μm; S) and number of vessel junctions (T) in Co versus Mut hearts at E16.5. Data represent mean ± SEM; n = 5 hearts per group. No significant differences were determined using an unpaired, two-tailed Student's t-test. All scale bars 100 μm.

bioRxiv preprint doi: https://doi.org/10.1101/2020.06.30.179952; this version posted July 2, 2020. The copyright holder for this preprint (which was not certified by peer review) is the author/funder, who has granted bioRxiv a license to display the preprint in perpetuity. It is made available under aCC-BY-NC-ND 4.0 International license.

Fig. 6. Ablation of the *Cx3cr1*$^{+}$ lineage disrupts cardiac lymphatic remodeling. (A-H) Whole-mount immunostaining for LYVE-1 (green) to visualize the sub-epicardial lymphatic plexus in both the dorsal and ventral aspects of E16.5 hearts-derived from littermate control (co; A-D) or *Cx3cr1-CreER;R26R-DTA* embryos (Mut; E-H), tamoxifen-induced at E12.5. (B,D,F,H) Magnified views of boxes shown in (A,C,E,G). (I,J) Quantification of total vessel length (μm; I) and number of lymphatic vessel junctions (J) in Co versus Mut hearts at E16.5. Data represent mean ± SEM; Co, n = 8 hearts; Mut, n = 7 hearts; three independent experiments. Significant differences (p values) were calculated using an unpaired, two-tailed Student's t-test (*$p \leq 0.05$). (K-R) Whole-mount immunostaining for EMCN (red) to visualize the sub-epicardial coronary vessels (capillaries and veins) in both the dorsal and ventral aspects of E16.5 hearts-derived from littermate control (co; K-N) or *Cx3cr1-CreER;R26R-DTA* embryos (Mut; O-R), tamoxifen-induced at E12.5. (L,N,P,R) Magnified views of boxes shown in (K,M,O,Q). White asterisks indicate patterning defects, i.e. an extra branch, of the coronary veins on the dorsal and ventral aspects of *Cx3cr1-CreER;R26R-DTA* hearts (compared O,Q with K,M), akin to *Pu.1*-null and *Csf1r-CreER;R26R-DTA* hearts (compared to Figs 3,5). (S,T) Quantification of total vessel length (μm; S) and number of vessel junctions (T) in Co versus Mut hearts at E16.5. Data represent mean ± SEM; Co, n = 8 hearts; Mut, n = 7 hearts. No significant differences were determined using an unpaired, two-tailed Student's t-test. All scale bars 100 μm.

bioRxiv preprint doi: https://doi.org/10.1101/2020.06.30.179952; this version posted July 2, 2020. The copyright holder for this preprint (which was not certified by peer review) is the author/funder, who has granted bioRxiv a license to display the preprint in perpetuity. It is made available under aCC-BY-NC-ND 4.0 International license.

Fig. 7. Macrophages promote lymphatic cell plexus formation and sprouting. (A-F) Representative frames of time-lapse experiments using primary human lymphatic endothelial cells (hLECs; phase-contrast) co-cultured with human iPS-derived macrophages labelled with RFP (red), showing close association between macrophages and LECs and a change in macrophage cell morphology (white arrowheads) contacting the expanding lymphatic plexus to facilitate LEC tube formation. (G-K) DAPI (blue), CD68 (green) and Phalloidin (red) staining of primary hLEC and hiPSC-macrophage co-cultures. (K) Magnified view of box shown in (J). (L-N) Representative staining of lymphatic capillary sprouting from beads coated with primary hLECs only (green; control medium; L) or co-cultured with hiPSC-derived macrophages-RFP (red; +macrophages; M). (N) Magnified view of box shown in (M). (O,P) Quantification of % sprouting activity defined as (number capillary sprouts/number of beads) x 100. Data was normalized against the control group. Data represent mean ± SEM; Control, n = 6; +Macrophages, n = 6; HAase 30U/mL, n = 3; siControl, n = 3; siCD18 #1, n = 3; siCD18 #2, n = 3 independent experiments, with three replicates/experiment. Significant differences (p values) were calculated using one-way ANOVA followed up by the Tukey's multiple comparison test (***$p \leq 0.001$). (Q-V) Representative staining of lymphatic capillary sprouting from hLECs aggregates/spheroids only (green; control medium; Q) or co-cultured with hiPSC-derived macrophages-RFP (red; +macrophages; R,T), hiPSC-derived macrophages-RFP pre-treated with HAase 30 U/mL (S), or co-cultured with hiPSC-derived macrophages-RFP pre-treated with siRNA oligonucleotides against *ITGB2*/*CD18* (siCD18 #1, U; siCD18 #2, V). (W,X) Quantification of % sprouting activity defined as (number capillary sprouts/number of beads) x 100. Data was normalized against the control group. Data represent mean ± SEM; Control, n = 5; +Macrophages, n = 4; HAase 30U/mL, n = 4; siControl, n = 3; siCD18 #1, n = 3; siCD18 #2, n = 3 independent experiments, with three replicates/ experiment. Significant differences (p

bioRxiv preprint doi: https://doi.org/10.1101/2020.06.30.179952; this version posted July 2, 2020. The copyright holder for this preprint (which was not certified by peer review) is the author/funder, who has granted bioRxiv a license to display the preprint in perpetuity. It is made available under aCC-BY-NC-ND 4.0 International license.

885 values) were calculated using one-way ANOVA followed up by the Tukey's multiple
886 comparison test (**$p \leq 0.01$; ***$p \leq 0.001$). All scale bars 100 μm, except N 50 μm and Q
887 250 μm.
888

bioRxiv preprint doi: https://doi.org/10.1101/2020.06.30.179952; this version posted July 2, 2020. The copyright holder for this preprint (which was not certified by peer review) is the author/funder, who has granted bioRxiv a license to display the preprint in perpetuity. It is made available under aCC-BY-NC-ND 4.0 International license.

SUPPLEMENTARY FIGURE LEGENDS

Fig. S1. Tissue-resident macrophages are present in the developing murine heart at E10.5. (A) UMAP plot demonstrating the different major clusters in the E10.5 heart scRNA-seq dataset (total 12,535 cells, n = 3 batches). (B) Dot plot showing proportion of cells in each cluster expressing selected genes. Dot size represents percentage of cells expressing, and color scale indicates average expression level. (C-E) Whole-mount immunostaining for GFP (green), and PECAM-1 (red) to visualize tissue-resident macrophages in the sinus venosus and ventricular surface of hearts-derived from *Cx3cr1*$^{GFP/+}$ embryos at E10.5. AvCu, atrioventricular cushion; CM_A, atrial cardiomyocytes; CM_AVC, atrioventricular canal cardiomyocytes; CM_OFT, cardiomyocytes of outflow tract; CM_Prol, proliferative cardiomyocytes; CM_S, septal cardiomyocytes; CM_SV, sinus venosus cardiomyocytes; CM_Trab, trabecular cardiomyocytes; CM_V, ventricular cardiomyocytes; Endo, endocardial cells; EndoMT, endocardial epithelial-to-mesenchymal transition; Epi, epithelial cells; Mes, mesenchyme; RBC, red blood cells; SHF, second heart field. Scale bar 100 μm

bioRxiv preprint doi: https://doi.org/10.1101/2020.06.30.179952; this version posted July 2, 2020. The copyright holder for this preprint (which was not certified by peer review) is the author/funder, who has granted bioRxiv a license to display the preprint in perpetuity. It is made available under aCC-BY-NC-ND 4.0 International license.

Fig. S2. Loss of macrophages is not associated with hyperproliferation of the cardiac lymphatic endothelium. (A,B) Representative flow cytometry histograms of cells isolated from control (Co) and *Pu.1*$^{-/-}$ hearts at E14.5 labeled against CD45 and CD11b (A) or F4/80 and CD11b markers (B). (C,D) Quantification of the myeloid (C), defined as CD45^{+}CD11b^{+}, and macrophage populations, defined as CD45^{+}CD11b^{+}F4/80^{+} (D) residing in Co versus *Pu.1*$^{-/-}$ hearts at E14.5. Data represent mean ± SEM; n = 4 hearts per group. Significant differences (p values) were calculated using an unpaired, two-tailed Student's t-test (**$p \leq$ 0.01). (E,F) Histological characterization of control and *Pu.1*$^{-/-}$ hearts at embryonic day (E) 16.5 using Hematoxylin & Eosin staining. (G-N) Whole-mount immunofluorescent staining for phospho-histone H3 (pH3; green) and PROX1 (red) in control (Co; G-J) and *Pu.1*$^{-/-}$ hearts (K-N) at E16.5. All scale bars 100 μm, except E 1mm.

bioRxiv preprint doi: https://doi.org/10.1101/2020.06.30.179952; this version posted July 2, 2020. The copyright holder for this preprint (which was not certified by peer review) is the author/funder, who has granted bioRxiv a license to display the preprint in perpetuity. It is made available under aCC-BY-NC-ND 4.0 International license.

916 **Fig. S3. Human induced pluripotent stem cell (hiPS)-derived macrophages display HA**
917 **on their cell surface, express HA-binding proteins and adhesion receptor CD18/CD11b**
918 **but lack the expression of *VEGFC*.** (A) Marker expression analysis by qRT-PCR using
919 RNA isolated from hiPS-macrophages. Data presented as mean ± SEM; n = 6 independent
920 experiments, with three replicates/experiment. (B-D) Representative HA staining (green) on
921 hiPSC-derived macrophages-RFP (red) under control conditions (B) or following incubation
922 with HAase 15 U/mL (C) and HAase 30 U/mL (D). DAPI (blue) labels the nuclear DNA.
923 Note the loss of cell surface (glycocalyx)-associated HA following treatment with HAase 30
924 U/mL. (E) *ITGB2* and (F) *ITGAM* expression analysis by qRT-PCR using RNA isolated from
925 control hiPS-macrophages (macrophages) or hiPS-macrophages treated with control siRNA
926 or siRNA oligonucleotides against *ITGB2*/*CD18* (two independent siRNA sequences were
927 used; siCD18 #1 and siCD18 #2). Data presented as mean ± SEM; n = 6 independent
928 experiments, with three replicates/experiment. Significant differences (p values) were
929 calculated using one-way ANOVA followed up by the Tukey's multiple comparison test
930 (****$p \leq 0.0001$). All scale bars 200 μm.
931

bioRxiv preprint doi: https://doi.org/10.1101/2020.06.30.179952; this version posted July 2, 2020. The copyright holder for this preprint (which was not certified by peer review) is the author/funder, who has granted bioRxiv a license to display the preprint in perpetuity. It is made available under aCC-BY-NC-ND 4.0 International license.

Fig. S4. Tissue-resident macrophages in the developing mouse heart display hyaluronan on their cell surface and lack expression of VEGF-C. (A-F) Whole-hearts from *Cx3cr1-GFP* embryos were analyzed for GFP (green), LYVE-1 (red) and VEGF-C (white) expression at E16.5. (B-F) Magnified views of box shown in (A). Note VEGF-C co-localization with LYVE-1 on lymphatic endothelium, but not on LYVE-1 and GFP co-expressing macrophages. (G-J) GFP (green) and VEGF-C (red) immunostaining of tissue sections derived from E16.5 hearts documenting lack of expression of VEGF-C in CX3CR1-GFP+ ventricular/subepicardial macrophages (G,H) and enrichment for VEGF-C in the coronary stems (white arrows; I, J). (H,J) Magnified views of boxes shown in (G,I). (K-P) Whole-hearts from *Cx3cr1-GFP* embryos were analyzed for GFP (green), HA (red) and LYVE-1 (white) expression at E16.5. (L-P) Magnified views of box shown in (K). Note HA colocalization with GFP and LYVE-1 in tissue-resident macrophages located in the subepicardial space, contiguous to the expanding lymphatic vasculature (white arrowheads in L). (Q-T) GFP (green), HA (red) and LYVE-1 (white) immunostaining of tissue sections derived from E16.5 hearts indicating expression of HA in CX3CR1-GFP+ subepicardial macrophages (white arrowheads in Q). DAPI (blue) labels nuclear DNA. LV, left ventricle; OFT, outflow tract. All scale bars100 μm, except H 25 μm and J,Q 50 μm.

bioRxiv preprint doi: https://doi.org/10.1101/2020.06.30.179952; this version posted July 2, 2020. The copyright holder for this preprint (which was not certified by peer review) is the author/funder, who has granted bioRxiv a license to display the preprint in perpetuity. It is made available under aCC-BY-NC-ND 4.0 International license.

950 **Movie S1.** Time-lapse imaging of tube formation in co-cultures of human primary lymphatic

951 endothelial cells (phase contrast) and human-iPS-derived macrophages expressing RFP.

952

bioRxiv preprint doi: https://doi.org/10.1101/2020.06.30.179952; this version posted July 2, 2020. The copyright holder for this preprint (which was not certified by peer review) is the author/funder, who has granted bioRxiv a license to display the preprint in perpetuity. It is made available under aCC-BY-NC-ND 4.0 International license.

953 **References**

954 Aurora, A. B., Porrello, E. R., Tan, W., Mahmoud, A. I., Hill, J. A., Bassel-Duby, R., Sadek,
955 H. A. and Olson, E. N. (2014). Macrophages are required for neonatal heart regeneration. *J*
956 *Clin Invest, 124*(3), 1382-1392. doi:10.1172/JCI72181

957 Becht, E., McInnes, L., Healy, J., Dutertre, C. A., Kwok, I. W. H., Ng, L. G., Ginhoux, F. and
958 Newell, E. W. (2018). Dimensionality reduction for visualizing single-cell data using UMAP.
959 *Nat Biotechnol*. doi:10.1038/nbt.4314

960 Benz, C., Martins, V. C., Radtke, F. and Bleul, C. C. (2008). The stream of precursors that
961 colonizes the thymus proceeds selectively through the early T lineage precursor stage of T
962 cell development. *J Exp Med, 205*(5), 1187-1199. doi:10.1084/jem.20072168

963 Boyer, S. W., Schroeder, A. V., Smith-Berdan, S. and Forsberg, E. C. (2011). All
964 hematopoietic cells develop from hematopoietic stem cells through Flk2/Flt3-positive
965 progenitor cells. *Cell Stem Cell, 9*(1), 64-73. doi:10.1016/j.stem.2011.04.021

966 Brachtendorf, G., Kuhn, A., Samulowitz, U., Knorr, R., Gustafsson, E., Potocnik, A. J.,
967 Fassler, R. and Vestweber, D. (2001). Early expression of endomucin on endothelium of the
968 mouse embryo and on putative hematopoietic clusters in the dorsal aorta. *Dev Dyn, 222*(3),
969 410-419. doi:10.1002/dvdy.1199

970 Buchrieser, J., James, W. and Moore, M. D. (2017). Human Induced Pluripotent Stem Cell-
971 Derived Macrophages Share Ontogeny with MYB-Independent Tissue-Resident
972 Macrophages. *Stem Cell Reports, 8*(2), 334-345. doi:10.1016/j.stemcr.2016.12.020

973 Butler, A., Hoffman, P., Smibert, P., Papalexi, E. and Satija, R. (2018). Integrating single-cell
974 transcriptomic data across different conditions, technologies, and species. *Nat Biotechnol,*
975 *36*(5), 411-420. doi:10.1038/nbt.4096

976 Camenisch, T. D., Spicer, A. P., Brehm-Gibson, T., Biesterfeldt, J., Augustine, M. L.,
977 Calabro, A., Jr., Kubalak, S., Klewer, S. E. and McDonald, J. A. (2000). Disruption of

bioRxiv preprint doi: https://doi.org/10.1101/2020.06.30.179952; this version posted July 2, 2020. The copyright holder for this preprint (which was not certified by peer review) is the author/funder, who has granted bioRxiv a license to display the preprint in perpetuity. It is made available under aCC-BY-NC-ND 4.0 International license.

978 hyaluronan synthase-2 abrogates normal cardiac morphogenesis and hyaluronan-mediated
979 transformation of epithelium to mesenchyme. *J Clin Invest*, *106*(3), 349-360.
980 doi:10.1172/JCI10272
981 Chen, H. I., Sharma, B., Akerberg, B. N., Numi, H. J., Kivela, R., Saharinen, P., Aghajanian,
982 H., McKay, A. S., Bogard, P. E., Chang, A. H., Jacobs, A. H., Epstein, J. A., Stankunas, K.,
983 Alitalo, K. andRed-Horse, K. (2014). The sinus venosus contributes to coronary vasculature
984 through VEGFC-stimulated angiogenesis. *Development*, *141*(23), 4500-4512.
985 doi:10.1242/dev.113639
986 de Soysa, T. Y., Ranade, S. S., Okawa, S., Ravichandran, S., Huang, Y., Salunga, H. T.,
987 Schricker, A., Del Sol, A., Gifford, C. A. and Srivastava, D. (2019). Single-cell analysis of
988 cardiogenesis reveals basis for organ-level developmental defects. *Nature*, *572*(7767), 120-
989 124. doi:10.1038/s41586-019-1414-x
990 Dongaonkar, R. M., Stewart, R. H., Geissler, H. J. and Laine, G. A. (2010). Myocardial
991 microvascular permeability, interstitial oedema, and compromised cardiac function.
992 *Cardiovasc Res*, *87*(2), 331-339. doi:10.1093/cvr/cvq145
993 Eng, T. C., Chen, W., Okuda, K. S., Misa, J. P., Padberg, Y., Crosier, K. E., Crosier, P. S.,
994 Hall, C. J., Schulte-Merker, S., Hogan, B. M. andAstin, J. W. (2019). Zebrafish facial
995 lymphatics develop through sequential addition of venous and non-venous progenitors.
996 *EMBO Rep*, *20*(5). doi:10.15252/embr.201847079
997 Fantin, A., Vieira, J. M., Gestri, G., Denti, L., Schwarz, Q., Prykhozhij, S., Peri, F., Wilson,
998 S. W. and Ruhrberg, C. (2010). Tissue macrophages act as cellular chaperones for vascular
999 anastomosis downstream of VEGF-mediated endothelial tip cell induction. *Blood*, *116*(5),
1000 829-840. doi:10.1182/blood-2009-12-257832
1001 Flaht-Zabost, A., Gula, G., Ciszek, B., Czarnowska, E., Jankowska-Steifer, E., Madej, M.,
1002 Niderla-Bielinska, J., Radomska-Lesniewska, D. and Ratajska, A. (2014). Cardiac mouse

bioRxiv preprint doi: https://doi.org/10.1101/2020.06.30.179952; this version posted July 2, 2020. The copyright holder for this preprint (which was not certified by peer review) is the author/funder, who has granted bioRxiv a license to display the preprint in perpetuity. It is made available under aCC-BY-NC-ND 4.0 International license.

1003 lymphatics: developmental and anatomical update. *Anat Rec (Hoboken), 297*(6), 1115-1130.
1004 doi:10.1002/ar.22912
1005 Gahmberg, C. G. (1997). Leukocyte adhesion: CD11/CD18 integrins and intercellular
1006 adhesion molecules. *Curr Opin Cell Biol, 9*(5), 643-650. doi:10.1016/s0955-0674(97)80117-
1007 2
1008 Gale, N. W., Prevo, R., Espinosa, J., Ferguson, D. J., Dominguez, M. G., Yancopoulos, G.
1009 D., Thurston, G. and Jackson, D. G. (2007). Normal lymphatic development and function in
1010 mice deficient for the lymphatic hyaluronan receptor LYVE-1. *Mol Cell Biol, 27*(2), 595-604.
1011 doi:10.1128/MCB.01503-06
1012 Gancz, D., Raftrey, B. C., Perlmoter, G., Marin-Juez, R., Semo, J., Matsuoka, R. L., Karra,
1013 R., Raviv, H., Moshe, N., Addadi, Y., Golani, O., Poss, K. D., Red-Horse, K., Stainier, D. Y.
1014 andYaniv, K. (2019). Distinct origins and molecular mechanisms contribute to lymphatic
1015 formation during cardiac growth and regeneration. *Elife, 8*. doi:10.7554/eLife.44153
1016 Ginhoux, F., Greter, M., Leboeuf, M., Nandi, S., See, P., Gokhan, S., Mehler, M. F.,
1017 Conway, S. J., Ng, L. G., Stanley, E. R., Samokhvalov, I. M. andMerad, M. (2010). Fate
1018 mapping analysis reveals that adult microglia derive from primitive macrophages. *Science,*
1019 *330*(6005), 841-845. doi:10.1126/science.1194637
1020 Ginhoux, F. and Guilliams, M. (2016). Tissue-Resident Macrophage Ontogeny and
1021 Homeostasis. *Immunity, 44*(3), 439-449. doi:10.1016/j.immuni.2016.02.024
1022 Gomez Perdiguero, E., Klapproth, K., Schulz, C., Busch, K., Azzoni, E., Crozet, L., Garner,
1023 H., Trouillet, C., de Bruijn, M. F., Geissmann, F. andRodewald, H. R. (2015). Tissue-resident
1024 macrophages originate from yolk-sac-derived erythro-myeloid progenitors. *Nature,*
1025 *518*(7540), 547-551. doi:10.1038/nature13989
1026 Gordon, E. J., Rao, S., Pollard, J. W., Nutt, S. L., Lang, R. A. and Harvey, N. L. (2010).
1027 Macrophages define dermal lymphatic vessel calibre during development by regulating

bioRxiv preprint doi: https://doi.org/10.1101/2020.06.30.179952; this version posted July 2, 2020. The copyright holder for this preprint (which was not certified by peer review) is the author/funder, who has granted bioRxiv a license to display the preprint in perpetuity. It is made available under aCC-BY-NC-ND 4.0 International license.

lymphatic endothelial cell proliferation. *Development, 137*(22), 3899-3910. doi:10.1242/dev.050021

Graney, P. L., Ben-Shaul, S., Landau, S., Bajpai, A., Singh, B., Eager, J., Cohen, A., Levenberg, S. and Spiller, K. L. (2020). Macrophages of diverse phenotypes drive vascularization of engineered tissues. *Sci Adv, 6*(18), eaay6391. doi:10.1126/sciadv.aay6391

Gurevich, D. B., Severn, C. E., Twomey, C., Greenhough, A., Cash, J., Toye, A. M., Mellor, H. and Martin, P. (2018). Live imaging of wound angiogenesis reveals macrophage orchestrated vessel sprouting and regression. *EMBO J, 37*(13). doi:10.15252/embj.201797786

Haenseler, W., Sansom, S. N., Buchrieser, J., Newey, S. E., Moore, C. S., Nicholls, F. J., Chintawar, S., Schnell, C., Antel, J. P., Allen, N. D., Cader, M. Z., Wade-Martins, R., James, W. S. andCowley, S. A. (2017). A Highly Efficient Human Pluripotent Stem Cell Microglia Model Displays a Neuronal-Co-culture-Specific Expression Profile and Inflammatory Response. *Stem Cell Reports, 8*(6), 1727-1742. doi:10.1016/j.stemcr.2017.05.017

Hill, M. C., Kadow, Z. A., Li, L., Tran, T. T., Wythe, J. D. and Martin, J. F. (2019). A cellular atlas of Pitx2-dependent cardiac development. *Development, 146*(12). doi:10.1242/dev.180398

Hoeffel, G., Chen, J., Lavin, Y., Low, D., Almeida, F. F., See, P., Beaudin, A. E., Lum, J., Low, I., Forsberg, E. C., Poidinger, M., Zolezzi, F., Larbi, A., Ng, L. G., Chan, J. K., Greter, M., Becher, B., Samokhvalov, I. M., Merad, M. andGinhoux, F. (2015). C-Myb(+) erythro-myeloid progenitor-derived fetal monocytes give rise to adult tissue-resident macrophages. *Immunity, 42*(4), 665-678. doi:10.1016/j.immuni.2015.03.011

Hulsmans, M., Clauss, S., Xiao, L., Aguirre, A. D., King, K. R., Hanley, A., Hucker, W. J., Wulfers, E. M., Seemann, G., Courties, G., Iwamoto, Y., Sun, Y., Savol, A. J., Sager, H. B., Lavine, K. J., Fishbein, G. A., Capen, D. E., Da Silva, N., Miquerol, L., Wakimoto, H.,

bioRxiv preprint doi: https://doi.org/10.1101/2020.06.30.179952; this version posted July 2, 2020. The copyright holder for this preprint (which was not certified by peer review) is the author/funder, who has granted bioRxiv a license to display the preprint in perpetuity. It is made available under aCC-BY-NC-ND 4.0 International license.

1053 Seidman, C. E., Seidman, J. G., Sadreyev, R. I., Naxerova, K., Mitchell, R. N., Brown, D.,
1054 Libby, P., Weissleder, R., Swirski, F. K., Kohl, P., Vinegoni, C., Milan, D. J., Ellinor, P. T.
1055 andNahrendorf, M. (2017). Macrophages Facilitate Electrical Conduction in the Heart. *Cell, 169*(3), 510-522 e520. doi:10.1016/j.cell.2017.03.050
1057 Hume, D. A. and Gordon, S. (1983). Mononuclear phagocyte system of the mouse defined by
1058 immunohistochemical localization of antigen F4/80. Identification of resident macrophages
1059 in renal medullary and cortical interstitium and the juxtaglomerular complex. *J Exp Med, 157*(5), 1704-1709. doi:10.1084/jem.157.5.1704
1061 Iqbal, A. J., McNeill, E., Kapellos, T. S., Regan-Komito, D., Norman, S., Burd, S., Smart, N.,
1062 Machemer, D. E., Stylianou, E., McShane, H., Channon, K. M., Chawla, A. andGreaves, D.
1063 R. (2014). Human CD68 promoter GFP transgenic mice allow analysis of monocyte to
1064 macrophage differentiation in vivo. *Blood, 124*(15), e33-44. doi:10.1182/blood-2014-04-
1065 568691
1066 Jackson, D. G. (2019). Hyaluronan in the lymphatics: The key role of the hyaluronan receptor
1067 LYVE-1 in leucocyte trafficking. *Matrix Biol, 78-79*, 219-235.
1068 doi:10.1016/j.matbio.2018.02.001
1069 Johnson, L. A., Banerji, S., Lawrance, W., Gileadi, U., Prota, G., Holder, K. A., Roshorm, Y.
1070 M., Hanke, T., Cerundolo, V., Gale, N. W. andJackson, D. G. (2017). Dendritic cells enter
1071 lymph vessels by hyaluronan-mediated docking to the endothelial receptor LYVE-1. *Nat Immunol, 18*(7), 762-770. doi:10.1038/ni.3750
1073 Jung, S., Aliberti, J., Graemmel, P., Sunshine, M. J., Kreutzberg, G. W., Sher, A. and
1074 Littman, D. R. (2000). Analysis of fractalkine receptor CX(3)CR1 function by targeted
1075 deletion and green fluorescent protein reporter gene insertion. *Mol Cell Biol, 20*(11), 4106-
1076 4114. Retrieved from http://www.ncbi.nlm.nih.gov/pubmed/10805752

bioRxiv preprint doi: https://doi.org/10.1101/2020.06.30.179952; this version posted July 2, 2020. The copyright holder for this preprint (which was not certified by peer review) is the author/funder, who has granted bioRxiv a license to display the preprint in perpetuity. It is made available under aCC-BY-NC-ND 4.0 International license.

1077 Kasaai, B., Caolo, V., Peacock, H. M., Lehoux, S., Gomez-Perdiguero, E., Luttun, A. and
1078 Jones, E. A. (2017). Erythro-myeloid progenitors can differentiate from endothelial cells and
1079 modulate embryonic vascular remodeling. *Sci Rep, 7*, 43817. doi:10.1038/srep43817
1080 Klotz, L., Norman, S., Vieira, J. M., Masters, M., Rohling, M., Dube, K. N., Bollini, S.,
1081 Matsuzaki, F., Carr, C. A. and Riley, P. R. (2015). Cardiac lymphatics are heterogeneous in
1082 origin and respond to injury. *Nature, 522*(7554), 62-67. doi:10.1038/nature14483
1083 Laine, G. A. and Allen, S. J. (1991). Left ventricular myocardial edema. Lymph flow,
1084 interstitial fibrosis, and cardiac function. *Circ Res, 68*(6), 1713-1721. Retrieved from
1085 https://www.ncbi.nlm.nih.gov/pubmed/2036720
1086 Lavine, K. J., Epelman, S., Uchida, K., Weber, K. J., Nichols, C. G., Schilling, J. D., Ornitz,
1087 D. M., Randolph, G. J. and Mann, D. L. (2014). Distinct macrophage lineages contribute to
1088 disparate patterns of cardiac recovery and remodeling in the neonatal and adult heart. *Proc*
1089 *Natl Acad Sci U S A, 111*(45), 16029-16034. doi:10.1073/pnas.1406508111
1090 Lawrance, W., Banerji, S., Day, A. J., Bhattacharjee, S. and Jackson, D. G. (2016). Binding
1091 of Hyaluronan to the Native Lymphatic Vessel Endothelial Receptor LYVE-1 Is Critically
1092 Dependent on Receptor Clustering and Hyaluronan Organization. *J Biol Chem, 291*(15),
1093 8014-8030. doi:10.1074/jbc.M115.708305
1094 Leid, J., Carrelha, J., Boukarabila, H., Epelman, S., Jacobsen, S. E. and Lavine, K. J. (2016).
1095 Primitive Embryonic Macrophages are Required for Coronary Development and Maturation.
1096 *Circ Res, 118*(10), 1498-1511. doi:10.1161/CIRCRESAHA.115.308270
1097 Lim, H. Y., Lim, S. Y., Tan, C. K., Thiam, C. H., Goh, C. C., Carbajo, D., Chew, S. H. S.,
1098 See, P., Chakarov, S., Wang, X. N., Lim, L. H., Johnson, L. A., Lum, J., Fong, C. Y.,
1099 Bongso, A., Biswas, A., Goh, C., Evrard, M., Yeo, K. P., Basu, R., Wang, J. K., Tan, Y.,
1100 Jain, R., Tikoo, S., Choong, C., Weninger, W., Poidinger, M., Stanley, E. R., Collin, M., Tan,
1101 N. S., Ng, L. G., Jackson, D. G., Ginhoux, F. andAngeli, V. (2018). Hyaluronan Receptor

bioRxiv preprint doi: https://doi.org/10.1101/2020.06.30.179952; this version posted July 2, 2020. The copyright holder for this preprint (which was not certified by peer review) is the author/funder, who has granted bioRxiv a license to display the preprint in perpetuity. It is made available under aCC-BY-NC-ND 4.0 International license.

1102 LYVE-1-Expressing Macrophages Maintain Arterial Tone through Hyaluronan-Mediated
1103 Regulation of Smooth Muscle Cell Collagen. *Immunity*, *49*(6), 1191.
1104 doi:10.1016/j.immuni.2018.12.009
1105 Lioux, G., Liu, X., Temino, S., Oxendine, M., Ayala, E., Ortega, S., Kelly, R. G., Oliver, G.
1106 and Torres, M. (2020). A Second Heart Field-Derived Vasculogenic Niche Contributes to
1107 Cardiac Lymphatics. *Dev Cell*, *52*(3), 350-363 e356. doi:10.1016/j.devcel.2019.12.006
1108 Lobov, I. B., Rao, S., Carroll, T. J., Vallance, J. E., Ito, M., Ondr, J. K., Kurup, S., Glass, D.
1109 A., Patel, M. S., Shu, W., Morrisey, E. E., McMahon, A. P., Karsenty, G. andLang, R. A.
1110 (2005). WNT7b mediates macrophage-induced programmed cell death in patterning of the
1111 vasculature. *Nature*, *437*(7057), 417-421. doi:10.1038/nature03928
1112 Luong, M. X., Tam, J., Lin, Q., Hagendoorn, J., Moore, K. J., Padera, T. P., Seed, B.,
1113 Fukumura, D., Kucherlapati, R. and Jain, R. K. (2009). Lack of lymphatic vessel phenotype
1114 in LYVE-1/CD44 double knockout mice. *J Cell Physiol*, *219*(2), 430-437.
1115 doi:10.1002/jcp.21686
1116 Manasek, F. J. (1969). Myocardial cell death in the embryonic chick ventricle. *J Embryol Exp*
1117 *Morphol*, *21*(2), 271-284. Retrieved from https://www.ncbi.nlm.nih.gov/pubmed/5822887
1118 Martinez-Corral, I., Ulvmar, M. H., Stanczuk, L., Tatin, F., Kizhatil, K., John, S. W., Alitalo,
1119 K., Ortega, S. and Makinen, T. (2015). Nonvenous origin of dermal lymphatic vasculature.
1120 *Circ Res*, *116*(10), 1649-1654. doi:10.1161/CIRCRESAHA.116.306170
1121 Maruyama, K., Asai, J., Ii, M., Thorne, T., Losordo, D. W. and D'Amore, P. A. (2007).
1122 Decreased macrophage number and activation lead to reduced lymphatic vessel formation
1123 and contribute to impaired diabetic wound healing. *Am J Pathol*, *170*(4), 1178-1191.
1124 doi:10.2353/ajpath.2007.060018

bioRxiv preprint doi: https://doi.org/10.1101/2020.06.30.179952; this version posted July 2, 2020. The copyright holder for this preprint (which was not certified by peer review) is the author/funder, who has granted bioRxiv a license to display the preprint in perpetuity. It is made available under aCC-BY-NC-ND 4.0 International license.

Maruyama, K., Miyagawa-Tomita, S., Mizukami, K., Matsuzaki, F. and Kurihara, H. (2019). Isl1-expressing non-venous cell lineage contributes to cardiac lymphatic vessel development. *Dev Biol, 452*(2), 134-143. doi:10.1016/j.ydbio.2019.05.002

Maruyama, K., Nakazawa, T., Cursiefen, C., Maruyama, Y., Van Rooijen, N., D'Amore, P. A. and Kinoshita, S. (2012). The maintenance of lymphatic vessels in the cornea is dependent on the presence of macrophages. *Invest Ophthalmol Vis Sci, 53*(6), 3145-3153. doi:10.1167/iovs.11-8010

McKercher, S. R., Torbett, B. E., Anderson, K. L., Henkel, G. W., Vestal, D. J., Baribault, H., Klemsz, M., Feeney, A. J., Wu, G. E., Paige, C. J. andMaki, R. A. (1996). Targeted disruption of the PU.1 gene results in multiple hematopoietic abnormalities. *EMBO J, 15*(20), 5647-5658. Retrieved from https://www.ncbi.nlm.nih.gov/pubmed/8896458

Ochsenbein, A. M., Karaman, S., Proulx, S. T., Goldmann, R., Chittazhathu, J., Dasargyri, A., Chong, C., Leroux, J. C., Stanley, E. R. and Detmar, M. (2016). Regulation of lymphangiogenesis in the diaphragm by macrophages and VEGFR-3 signaling. *Angiogenesis, 19*(4), 513-524. doi:10.1007/s10456-016-9523-8

Parkhurst, C. N., Yang, G., Ninan, I., Savas, J. N., Yates, J. R., 3rd, Lafaille, J. J., Hempstead, B. L., Littman, D. R. and Gan, W. B. (2013). Microglia promote learning-dependent synapse formation through brain-derived neurotrophic factor. *Cell, 155*(7), 1596-1609. doi:10.1016/j.cell.2013.11.030

Petz, A., Grandoch, M., Gorski, D. J., Abrams, M., Piroth, M., Schneckmann, R., Homann, S., Muller, J., Hartwig, S., Lehr, S., Yamaguchi, Y., Wight, T. N., Gorressen, S., Ding, Z., Kotter, S., Kruger, M., Heinen, A., Kelm, M., Godecke, A., Flogel, U. andFischer, J. W. (2019). Cardiac Hyaluronan Synthesis Is Critically Involved in the Cardiac Macrophage Response and Promotes Healing After Ischemia Reperfusion Injury. *Circ Res, 124*(10), 1433-1447. doi:10.1161/CIRCRESAHA.118.313285

bioRxiv preprint doi: https://doi.org/10.1101/2020.06.30.179952; this version posted July 2, 2020. The copyright holder for this preprint (which was not certified by peer review) is the author/funder, who has granted bioRxiv a license to display the preprint in perpetuity. It is made available under aCC-BY-NC-ND 4.0 International license.

Pexieder, T. (1975). Cell death in the morphogenesis and teratogenesis of the heart. *Adv Anat Embryol Cell Biol, 51*(3), 3-99. Retrieved from https://www.ncbi.nlm.nih.gov/pubmed/50000

Plein, A., Fantin, A., Denti, L., Pollard, J. W. and Ruhrberg, C. (2018). Erythro-myeloid progenitors contribute endothelial cells to blood vessels. *Nature, 562*(7726), 223-228. doi:10.1038/s41586-018-0552-x

Qian, B. Z., Li, J., Zhang, H., Kitamura, T., Zhang, J., Campion, L. R., Kaiser, E. A., Snyder, L. A. and Pollard, J. W. (2011). CCL2 recruits inflammatory monocytes to facilitate breast-tumour metastasis. *Nature, 475*(7355), 222-225. doi:10.1038/nature10138

Qian, B. Z. and Pollard, J. W. (2010). Macrophage diversity enhances tumor progression and metastasis. *Cell, 141*(1), 39-51. doi:10.1016/j.cell.2010.03.014

Ran, S. and Montgomery, K. E. (2012). Macrophage-mediated lymphangiogenesis: the emerging role of macrophages as lymphatic endothelial progenitors. *Cancers (Basel), 4*(3), 618-657. doi:10.3390/cancers4030618

Savani, R. C., Cao, G., Pooler, P. M., Zaman, A., Zhou, Z. and DeLisser, H. M. (2001). Differential involvement of the hyaluronan (HA) receptors CD44 and receptor for HA-mediated motility in endothelial cell function and angiogenesis. *J Biol Chem, 276*(39), 36770-36778. doi:10.1074/jbc.M102273200

Schulz, M. M., Reisen, F., Zgraggen, S., Fischer, S., Yuen, D., Kang, G. J., Chen, L., Schneider, G. and Detmar, M. (2012). Phenotype-based high-content chemical library screening identifies statins as inhibitors of in vivo lymphangiogenesis. *Proc Natl Acad Sci U S A, 109*(40), E2665-2674. doi:10.1073/pnas.1206036109

Scott, E. W., Simon, M. C., Anastasi, J. and Singh, H. (1994). Requirement of transcription factor PU.1 in the development of multiple hematopoietic lineages. *Science, 265*(5178), 1573-1577. doi:10.1126/science.8079170

bioRxiv preprint doi: https://doi.org/10.1101/2020.06.30.179952; this version posted July 2, 2020. The copyright holder for this preprint (which was not certified by peer review) is the author/funder, who has granted bioRxiv a license to display the preprint in perpetuity. It is made available under aCC-BY-NC-ND 4.0 International license.

1174 Shigeta, A., Huang, V., Zuo, J., Besada, R., Nakashima, Y., Lu, Y., Ding, Y., Pellegrini, M.,
1175 Kulkarni, R. P., Hsiai, T., Deb, A., Zhou, B., Nakano, H. andNakano, A. (2019).
1176 Endocardially Derived Macrophages Are Essential for Valvular Remodeling. *Dev Cell, 48*(5),
1177 617-630 e613. doi:10.1016/j.devcel.2019.01.021
1178 Simoes, F. C. and Riley, P. R. (2018). The ontogeny, activation and function of the
1179 epicardium during heart development and regeneration. *Development, 145*(7).
1180 doi:10.1242/dev.155994
1181 Sorokin, S. P., McNelly, N. A. and Hoyt, R. F., Jr. (1994). Early development of
1182 macrophages in intact and organ cultured hearts of rat embryos. *Anat Rec, 239*(3), 306-314.
1183 doi:10.1002/ar.1092390309
1184 Stanczuk, L., Martinez-Corral, I., Ulvmar, M. H., Zhang, Y., Lavina, B., Fruttiger, M.,
1185 Adams, R. H., Saur, D., Betsholtz, C., Ortega, S., Alitalo, K., Graupera, M. andMakinen, T.
1186 (2015). cKit Lineage Hemogenic Endothelium-Derived Cells Contribute to Mesenteric
1187 Lymphatic Vessels. *Cell Rep, 10*(10), 1708-1721. doi:10.1016/j.celrep.2015.02.026
1188 Stevens, S. M., von Gise, A., VanDusen, N., Zhou, B. and Pu, W. T. (2016). Epicardium is
1189 required for cardiac seeding by yolk sac macrophages, precursors of resident macrophages of
1190 the adult heart. *Dev Biol, 413*(2), 153-159. doi:10.1016/j.ydbio.2016.03.014
1191 Stone, O. A. and Stainier, D. Y. R. (2019). Paraxial Mesoderm Is the Major Source of
1192 Lymphatic Endothelium. *Dev Cell*. doi:10.1016/j.devcel.2019.04.034
1193 Stremmel, C., Schuchert, R., Wagner, F., Thaler, R., Weinberger, T., Pick, R., Mass, E.,
1194 Ishikawa-Ankerhold, H. C., Margraf, A., Hutter, S., Vagnozzi, R., Klapproth, S., Frampton,
1195 J., Yona, S., Scheiermann, C., Molkentin, J. D., Jeschke, U., Moser, M., Sperandio, M.,
1196 Massberg, S., Geissmann, F. andSchulz, C. (2018). Yolk sac macrophage progenitors traffic
1197 to the embryo during defined stages of development. *Nat Commun, 9*(1), 75.
1198 doi:10.1038/s41467-017-02492-2

bioRxiv preprint doi: https://doi.org/10.1101/2020.06.30.179952; this version posted July 2, 2020. The copyright holder for this preprint (which was not certified by peer review) is the author/funder, who has granted bioRxiv a license to display the preprint in perpetuity. It is made available under aCC-BY-NC-ND 4.0 International license.

1199 Stuart, T., Butler, A., Hoffman, P., Hafemeister, C., Papalexi, E., Mauck, W. M., 3rd, Hao,
1200 Y., Stoeckius, M., Smibert, P. and Satija, R. (2019). Comprehensive Integration of Single-
1201 Cell Data. *Cell*, *177*(7), 1888-1902 e1821. doi:10.1016/j.cell.2019.05.031
1202 Sun, M., Puri, S., Mutoji, K. N., Coulson-Thomas, Y. M., Hascall, V. C., Jackson, D. G.,
1203 Gesteira, T. F. and Coulson-Thomas, V. J. (2019). Hyaluronan Derived From the Limbus is a
1204 Key Regulator of Corneal Lymphangiogenesis. *Invest Ophthalmol Vis Sci*, *60*(4), 1050-1062.
1205 doi:10.1167/iovs.18-25920
1206 Theret, M., Mounier, R. and Rossi, F. (2019). The origins and non-canonical functions of
1207 macrophages in development and regeneration. *Development*, *146*(9).
1208 doi:10.1242/dev.156000
1209 Triggs-Raine, B. and Natowicz, M. R. (2015). Biology of hyaluronan: Insights from genetic
1210 disorders of hyaluronan metabolism. *World J Biol Chem*, *6*(3), 110-120.
1211 doi:10.4331/wjbc.v6.i3.110
1212 Troegeler, A., Lastrucci, C., Duval, C., Tanne, A., Cougoule, C., Maridonneau-Parini, I.,
1213 Neyrolles, O. and Lugo-Villarino, G. (2014). An efficient siRNA-mediated gene silencing in
1214 primary human monocytes, dendritic cells and macrophages. *Immunol Cell Biol*, *92*(8), 699-
1215 708. doi:10.1038/icb.2014.39
1216 Ulvmar, M. H. and Makinen, T. (2016). Heterogeneity in the lymphatic vascular system and
1217 its origin. *Cardiovasc Res*, *111*(4), 310-321. doi:10.1093/cvr/cvw175
1218 van Wilgenburg, B., Browne, C., Vowles, J. and Cowley, S. A. (2013). Efficient, long term
1219 production of monocyte-derived macrophages from human pluripotent stem cells under
1220 partly-defined and fully-defined conditions. *PLoS One*, *8*(8), e71098.
1221 doi:10.1371/journal.pone.0071098
1222 Vieira, J. M., Norman, S., Villa Del Campo, C., Cahill, T. J., Barnette, D. N., Gunadasa-
1223 Rohling, M., Johnson, L. A., Greaves, D. R., Carr, C. A., Jackson, D. G. andRiley, P. R.

bioRxiv preprint doi: https://doi.org/10.1101/2020.06.30.179952; this version posted July 2, 2020. The copyright holder for this preprint (which was not certified by peer review) is the author/funder, who has granted bioRxiv a license to display the preprint in perpetuity. It is made available under aCC-BY-NC-ND 4.0 International license.

(2018). The cardiac lymphatic system stimulates resolution of inflammation following myocardial infarction. *J Clin Invest*. doi:10.1172/JCI97192

Yang, X., Zhao, L., Campos, M. M., Abu-Asab, M., Ortolan, D., Hotaling, N., Bharti, K. and Wong, W. T. (2020). CSF1R blockade induces macrophage ablation and results in mouse choroidal vascular atrophy and RPE disorganization. *Elife*, *9*. doi:10.7554/eLife.55564

Yona, S., Kim, K. W., Wolf, Y., Mildner, A., Varol, D., Breker, M., Strauss-Ayali, D., Viukov, S., Guilliams, M., Misharin, A., Hume, D. A., Perlman, H., Malissen, B., Zelzer, E. andJung, S. (2013). Fate mapping reveals origins and dynamics of monocytes and tissue macrophages under homeostasis. *Immunity*, *38*(1), 79-91. doi:10.1016/j.immuni.2012.12.001

Zudaire, E., Gambardella, L., Kurcz, C. and Vermeren, S. (2011). A computational tool for quantitative analysis of vascular networks. *PLoS One*, *6*(11), e27385. doi:10.1371/journal.pone.0027385

Figure 1

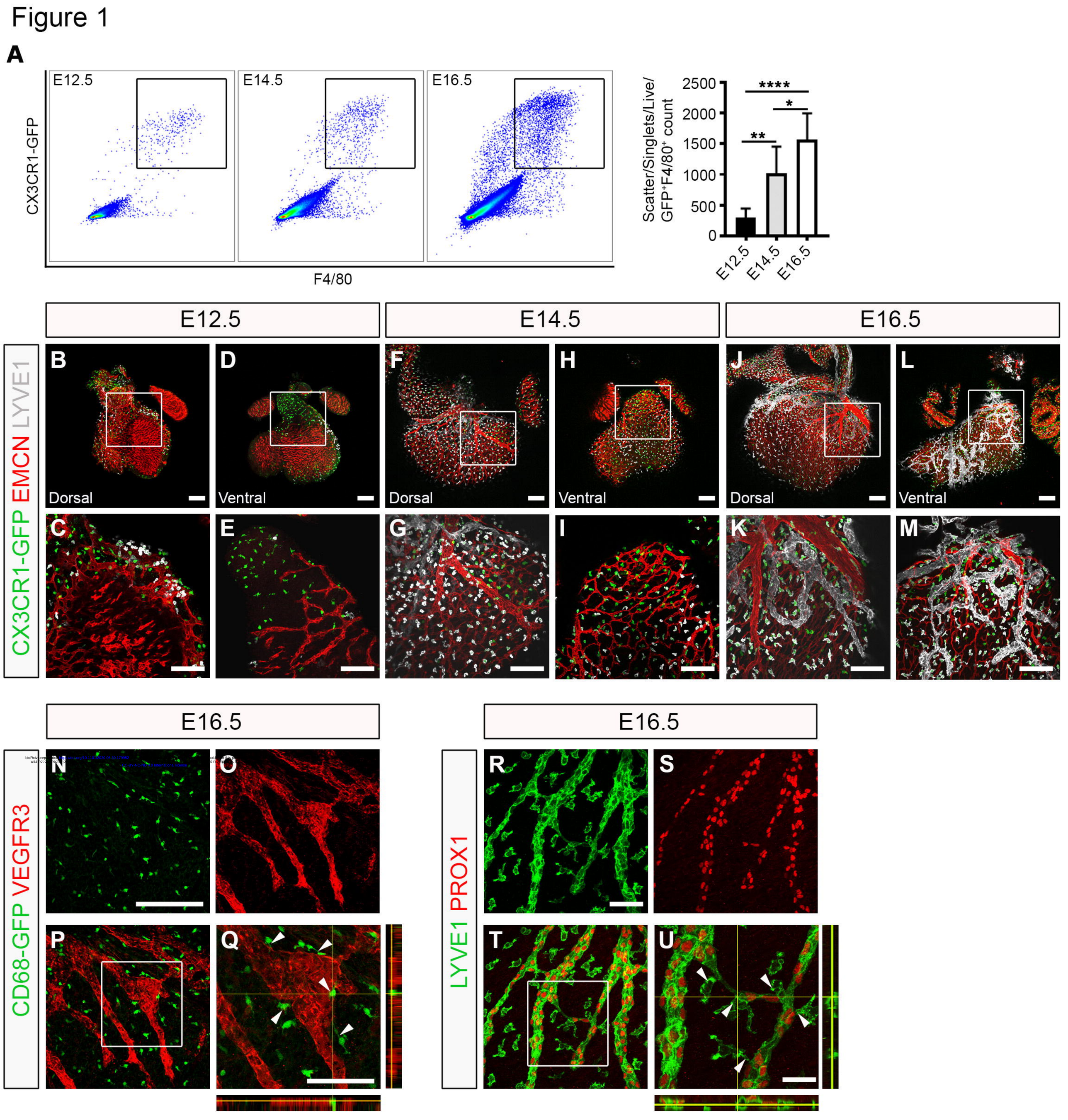

bioRxiv preprint doi: https://doi.org/10.1101/2020.06.30.179952 was not certified by peer review
CC-BY-NC-ND 4.0 International license

Figure 2

bioRxiv preprint doi: https://doi.org/10.1101/2020.06.30.179952; this version posted July 2, 2020. The copyright holder for this preprint (which was not certified by peer review) is the author/funder, who has granted bioRxiv a license to display the preprint in perpetuity. It is made available under aCC-BY-NC-ND 4.0 International license.

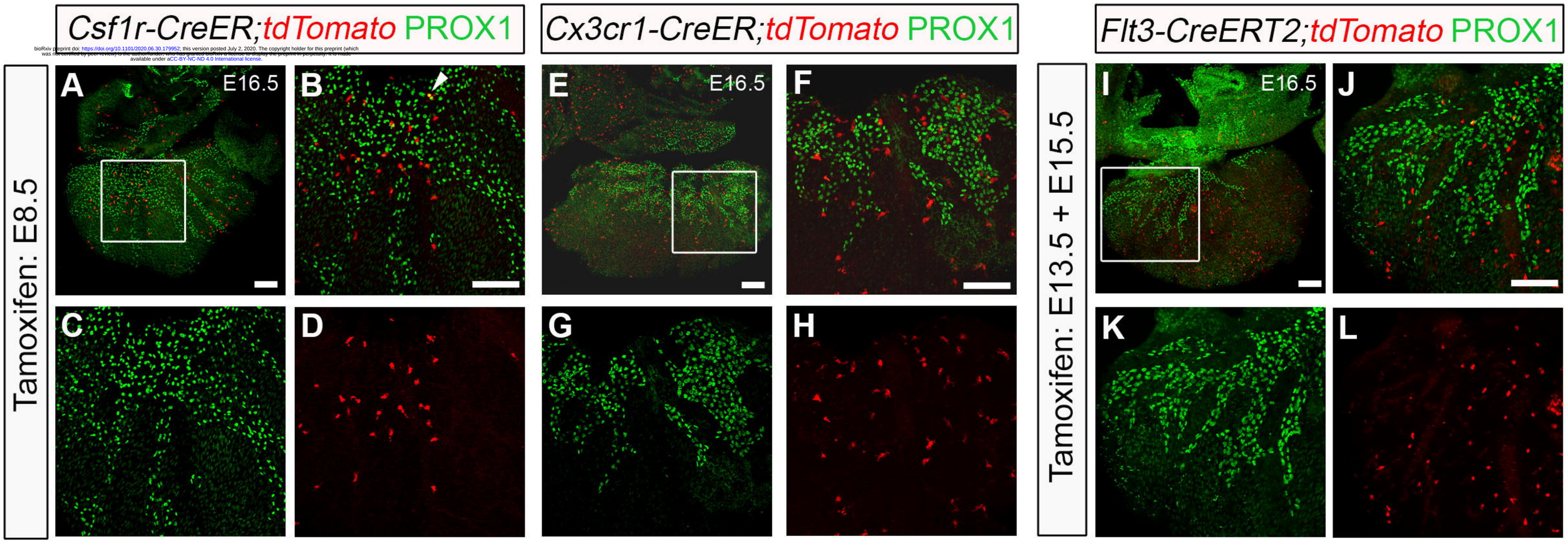

Figure 3

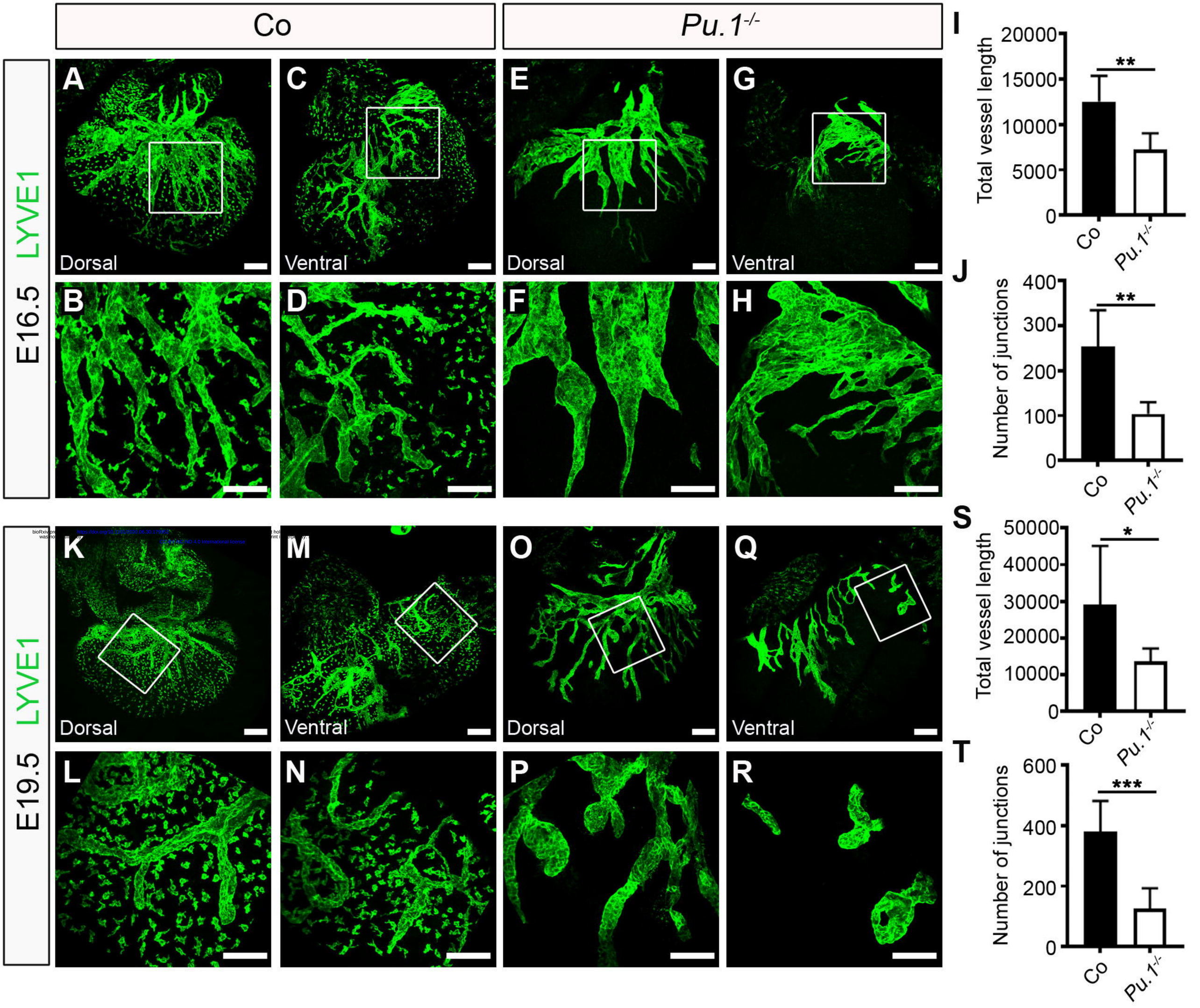

bioRxiv preprint https://doi.org/10.1101/2020.06.30.179952 was not certified by peer review
CC BY-NC-ND 4.0 International license

Figure 4

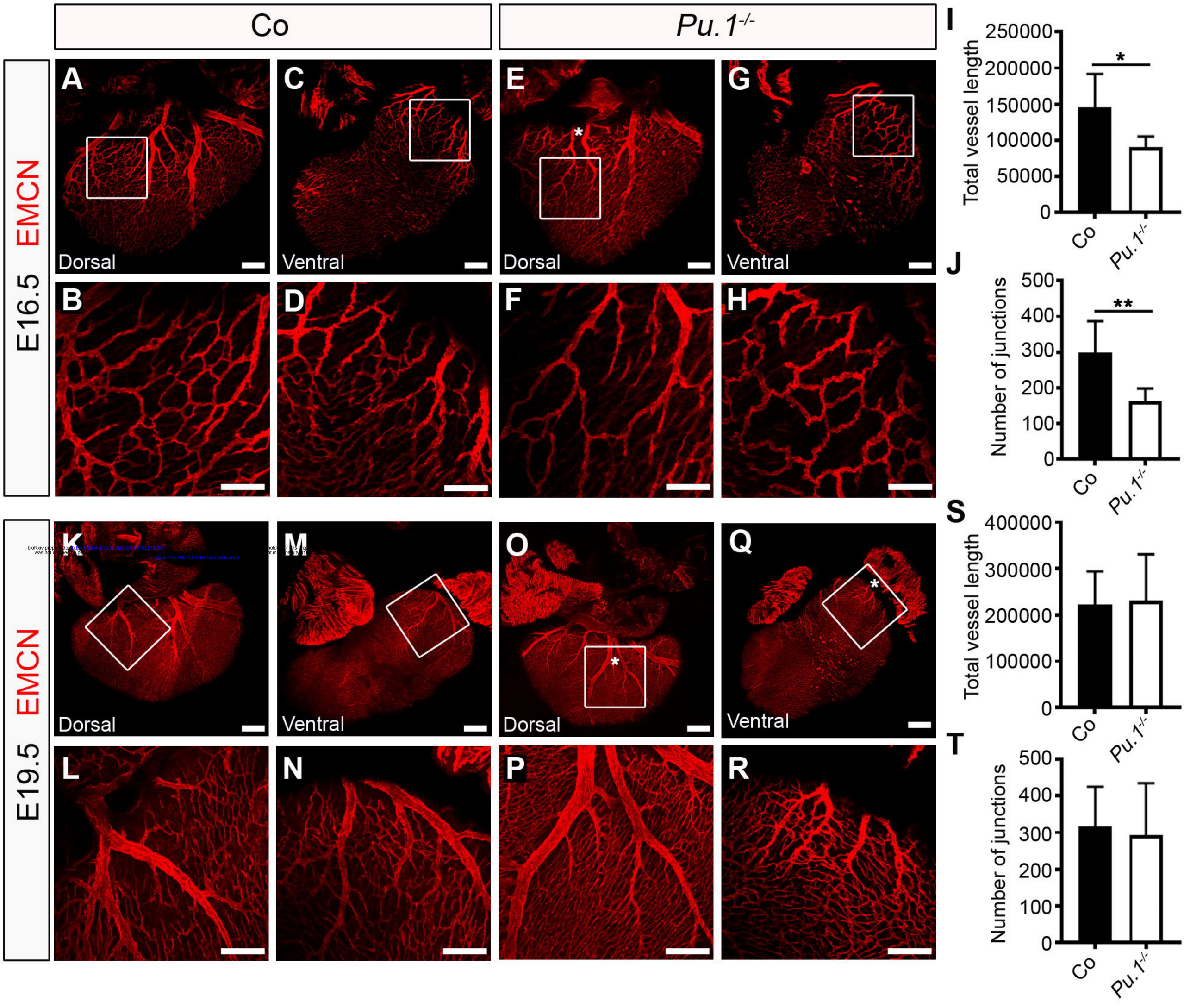

bioRxiv preprint doi: https://doi.org/10.1101/2020.03.30.179952 ; this version posted ... was not certified by peer review ... CC-BY-NC-ND 4.0 International license

Figure 5

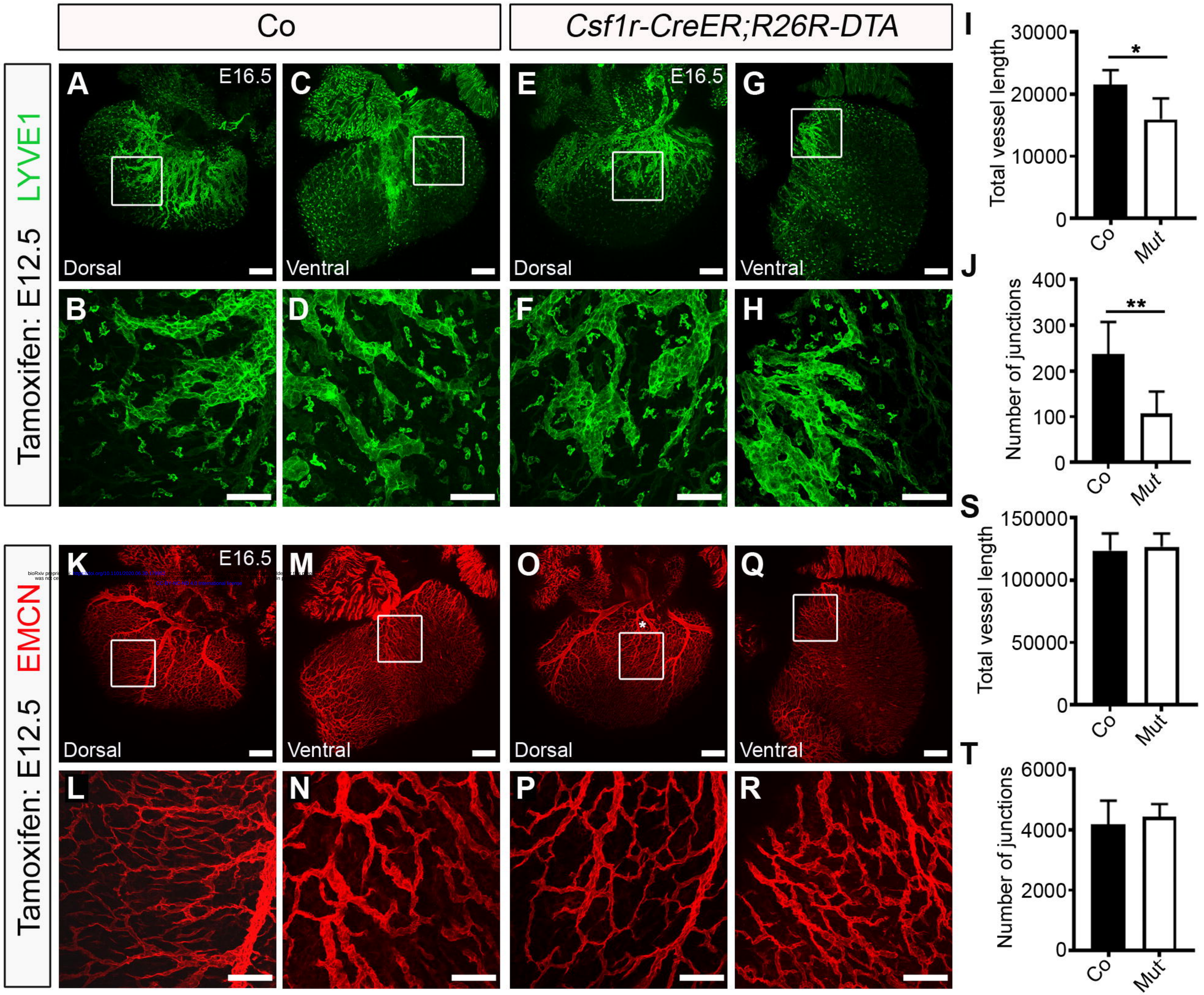
Co
Csf1r-CreER;R26R-DTA
Tamoxifen: E12.5 LYVE1
Tamoxifen: E12.5 EMCN
A
E16.5
Dorsal
B
C
Ventral
D
E
E16.5
Dorsal
F
G
Ventral
H
I
Total vessel length
30000
20000
10000
0
*
Co
Mut
J
Number of junctions
400
300
200
100
0
**
Co
Mut
S
Total vessel length
150000
100000
50000
0
Co
Mut
T
Number of junctions
6000
4000
2000
0
Co
Mut
K
E16.5
Dorsal
L
M
Ventral
N
O
Dorsal
*
P
Q
Ventral
R

Figure 6

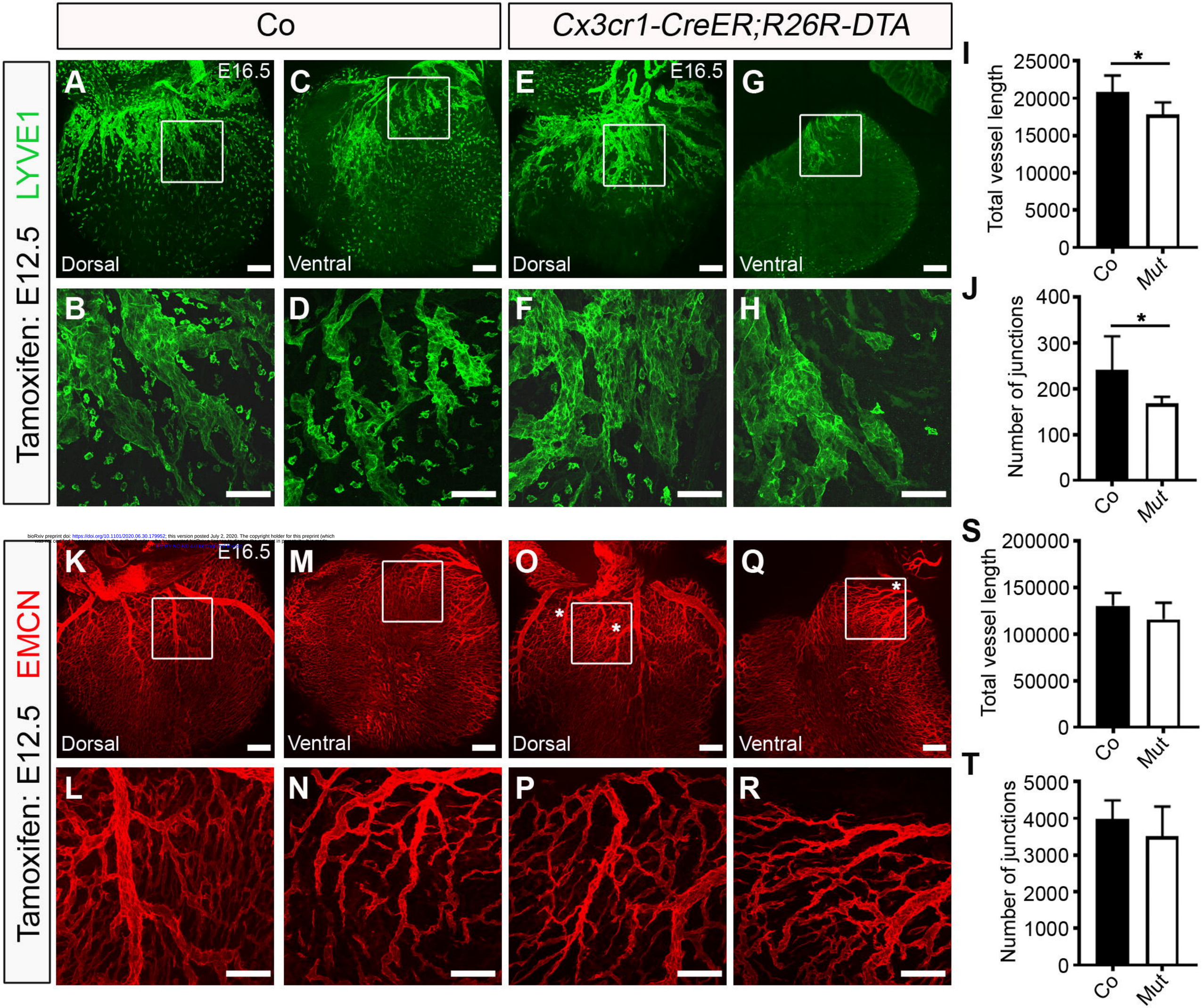

bioRxiv preprint doi: https://doi.org/10.1101/2020.06.30.179952; this version posted July 2, 2020. The copyright holder for this preprint (which was not certified by peer review) is the author/funder, who has granted bioRxiv a license to display the preprint in perpetuity. It is made available under CC-BY-NC-ND 4.0 International license.

Figure 7

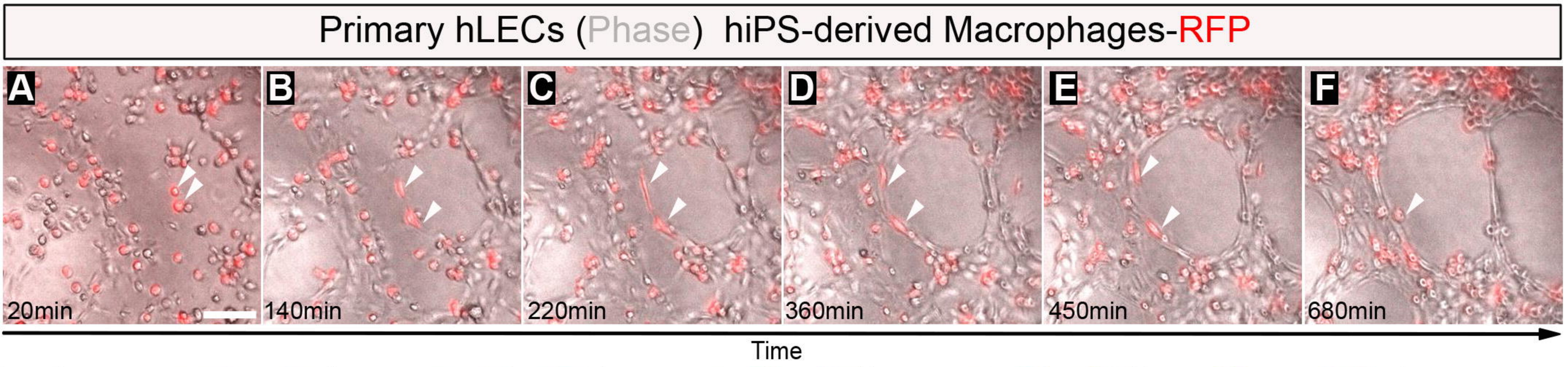
Primary hLECs (Phase) hiPS-derived Macrophages-RFP
A
B
C
D
E
F
20min
140min
220min
360min
450min
680min
Time

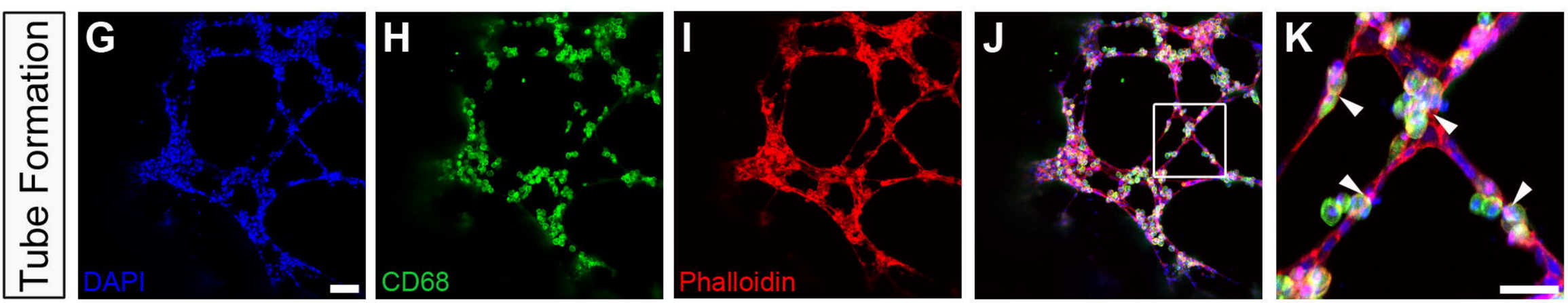
Tube Formation
G
H
I
J
K
DAPI
CD68
Phalloidin

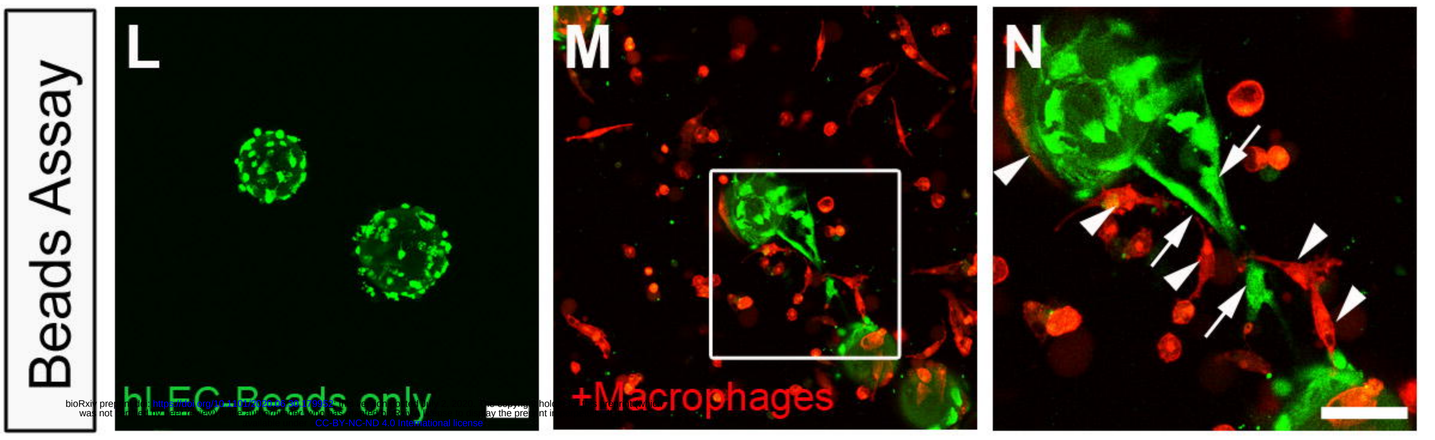
Beads Assay
L
M
N
hLEC Beads only
+Macrophages

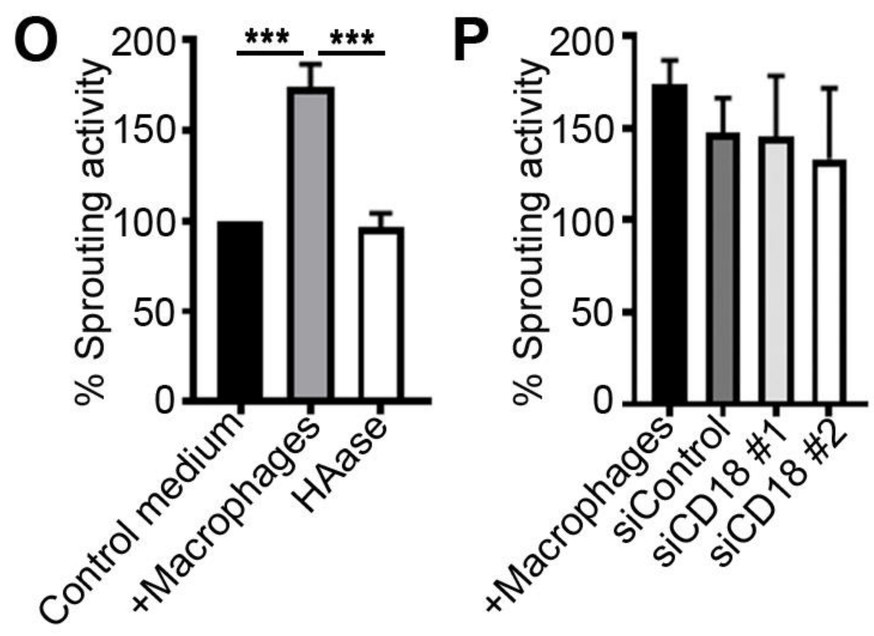
O
P
% Sprouting activity
200
150
100
50
0
***
***
Control medium
+Macrophages
HAase
+Macrophages
siControl
siCD18 #1
siCD18 #2

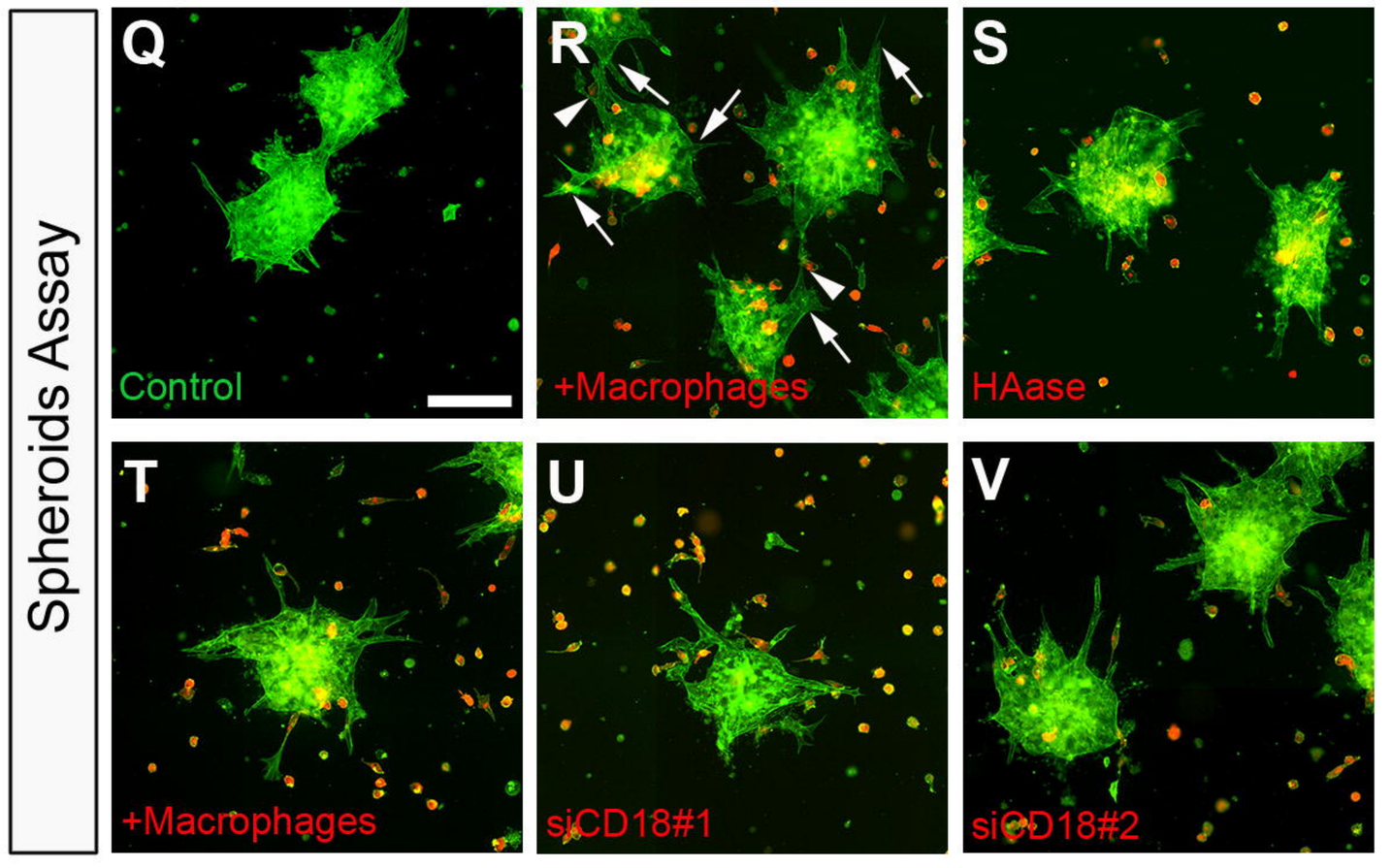
Spheroids Assay
Q
R
S
T
U
V
Control
+Macrophages
HAase
+Macrophages
siCD18#1
siCD18#2

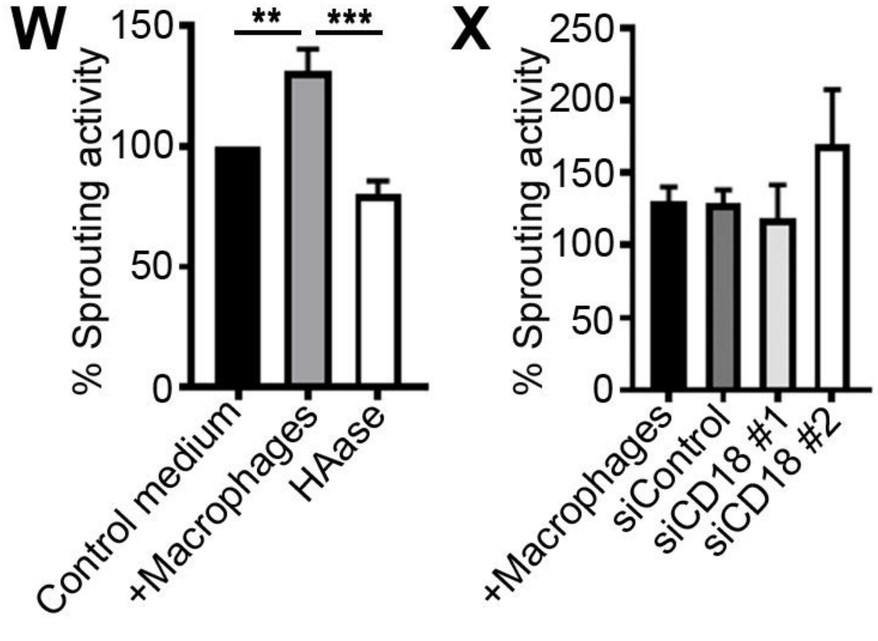
W
X
% Sprouting activity
150
100
50
0
250
200
150
100
50
0
**
***
Control medium
+Macrophages
HAase
+Macrophages
siControl
siCD18 #1
siCD18 #2